



**HAL**  
open science

## Shear wave anisotropy in the upper mantle beneath the Aegean related to internal deformation

D. Hatzfeld, E. Karagianni, I. Kassaras, A. Kiratzi, E. Louvari, H. Lyon-Caen, K. Makropoulos, P. Papadimitriou, G. Bock, K. Priestley

► **To cite this version:**

D. Hatzfeld, E. Karagianni, I. Kassaras, A. Kiratzi, E. Louvari, et al.. Shear wave anisotropy in the upper mantle beneath the Aegean related to internal deformation. *Journal of Geophysical Research : Solid Earth*, 2001, 106, pp.30,737-30,753. 10.1029/2001JB000387 . insu-03606670

**HAL Id: insu-03606670**

**<https://insu.hal.science/insu-03606670>**

Submitted on 12 Mar 2022

**HAL** is a multi-disciplinary open access archive for the deposit and dissemination of scientific research documents, whether they are published or not. The documents may come from teaching and research institutions in France or abroad, or from public or private research centers.

L'archive ouverte pluridisciplinaire **HAL**, est destinée au dépôt et à la diffusion de documents scientifiques de niveau recherche, publiés ou non, émanant des établissements d'enseignement et de recherche français ou étrangers, des laboratoires publics ou privés.

Copyright

## Shear wave anisotropy in the upper mantle beneath the Aegean related to internal deformation

D. Hatzfeld,<sup>1</sup> E. Karagianni,<sup>2</sup> I. Kassaras,<sup>3</sup> A. Kiratzi,<sup>2</sup> E. Louvari,<sup>2</sup> H. Lyon-Caen,<sup>4</sup> K. Makropoulos,<sup>3</sup> P. Papadimitriou,<sup>3</sup> G. Bock,<sup>5</sup> and K. Priestley<sup>6</sup>

**Abstract.** Seismic anisotropy, deduced from SKS splitting measured at 25 stations installed in the Aegean, does not show a homogeneous pattern. It is not restricted to the North Anatolian Fault but is distributed over a region several hundreds kilometers wide. Little anisotropy is observed in continental Greece or along the Hellenic arc; however, significant anisotropy is observed in the north Aegean Sea. Large values of delay times suggest that anisotropy is due to a long path within the upper mantle and to strong intrinsic anisotropy. Our results, both in fast polarization directions and in values of delay time, do not support the idea that anisotropy is associated with inherited tectonic fabric nor are they consistent with the present-day Aegean motion relative to an absolute frame. In contrast, the direction of fast polarization and the magnitude of delay times correlate well with the present-day strain rate observed at the surface deduced from both geodetic measurements and seismicity. This anisotropy is not horizontally restricted to major surface faults but is spread over a wide region.

### 1. Introduction

There are currently two conflicting views of how the continental lithosphere deforms. One view is that the lithosphere consists of essentially rigid blocks that float on the asthenosphere, are separated by lithospheric faults, and move because of forces that are applied on their edge [e.g., *Tapponnier et al.*, 1986; *Nur et al.*, 1986]. The other view holds that the lithosphere deforms as a continuum and the upper crust moves in response to tractions applied to its base [e.g., *England and McKenzie*, 1982; *Molnar*, 1988; *Bourne et al.*, 1997]. Most of the measurements used to distinguish between one view and the other consider deformation near the surface or within the shallow crust. They are related to fault kinematics [e.g., *Tapponnier et al.*, 1986], geodetic displacements [e.g., *Bourne et al.*, 1997], or earthquake mechanisms [e.g., *Jackson et al.*, 1992]. Very few observations sample the deformation of the lithosphere as a whole, making it difficult to determine if the lithosphere deforms in the same manner as the crust and whether faults that are seen at the surface also cut the mantle lithosphere.

Although the African and Eurasian lithospheric plates converge at a rate of  $\sim 1$  cm/yr, deformation of the Aegean is fast and intense (Figure 1), and convergence across the Hellenic Trench is  $>4$  cm/yr, as evidenced by geodetic measurements [e.g., *McClusky et al.*, 2000]. This high rate is partly due to the motion of the rigid Anatolian plate toward the west around a pole of rotation located in the eastern Mediterranean [e.g., *McKenzie*, 1978; *Le Pichon et al.*, 1995]. However, slight discrepancies in the displacements compared to those modeled by the rotation of a rigid plate around a

pole are observed in the Aegean and along the Hellenic arc [*Davies et al.*, 1997; *Kahle et al.*, 1998; *McClusky et al.*, 2000]. This implies that internal deformation affects the Aegean [*Le Pichon and Angelier*, 1979; *England et al.*, 1985; *Hatzfeld et al.*, 1997; *Meijer and Wortel*, 1997]. This internal deformation is certainly fast, as indicated by the existence of major active crustal faults, by the seismic activity, and by the thinning of the crust.

### 2. Data

Mantle seismic anisotropy is most probably related to the lattice-preferred orientation of anisotropic minerals (especially olivine) through deformation [*Nicolas and Christensen*, 1987; *Mainprice and Silver*, 1993; *Ben Ismail and Mainprice*, 1998]. In oceanic regions it is probably related to the mantle flow and therefore to the plate motion [*Tommasi et al.*, 1996]. In continental areas, however, it is thought to be related to internal deformation [*Silver*, 1996], although it is not clear how much has been frozen in by past tectonic activity and how much relates to recent, ongoing deformation. Seismic anisotropy would be parallel to the absolute plate motion [*Vinnik et al.*, 1992] if it is caused by “simple asthenospheric flow,” but many observations in continental areas indicate that significant small-scale variations of the fast polarization direction [e.g., *Wylegalla et al.*, 1999] are correlated to surface tectonics and support the idea of “vertically coherent deformation” [*Silver*, 1996]. The Aegean is a good place to test competing ideas of how the anisotropy originates because the surface strain varies widely over the region, the past deformation is reasonably well known and differs significantly from the present deformation, and we have a fair idea of the internal deformation or of the motion of the region relative to the asthenosphere. Thus we can test the relative contribution of past, inherited fabric, present asthenospheric flow, or present deformation toward observed seismic anisotropy.

Shear wave splitting is one of the most reliable methods of investigating mantle anisotropy. SKS, at the receiver, is radially polarized as an *SV* wave, and the time delay between the arrival times of the two split quasi-*S* waves and the orientation of the fast polarization gives information mainly about horizontal mantle anisotropy.

From January 1997 to July 1997, we maintained a network of 30 seismological stations across the Aegean to record tele-

<sup>1</sup>Laboratoire de Géophysique Interne et Tectonophysique, UJF-CNRS, Grenoble, France.

<sup>2</sup>Department of Geophysics, Aristotle University, Thessaloniki, Greece.

<sup>3</sup>Department of Geophysics, University of Athens, Athens, Greece.

<sup>4</sup>Laboratoire de Géologie, Ecole Normale Supérieure, Paris, France.

<sup>5</sup>GeoForschungsZentrum Potsdam, Potsdam, Germany.

<sup>6</sup>Bullard Laboratory, Madingley Rise, Cambridge, England, UK.

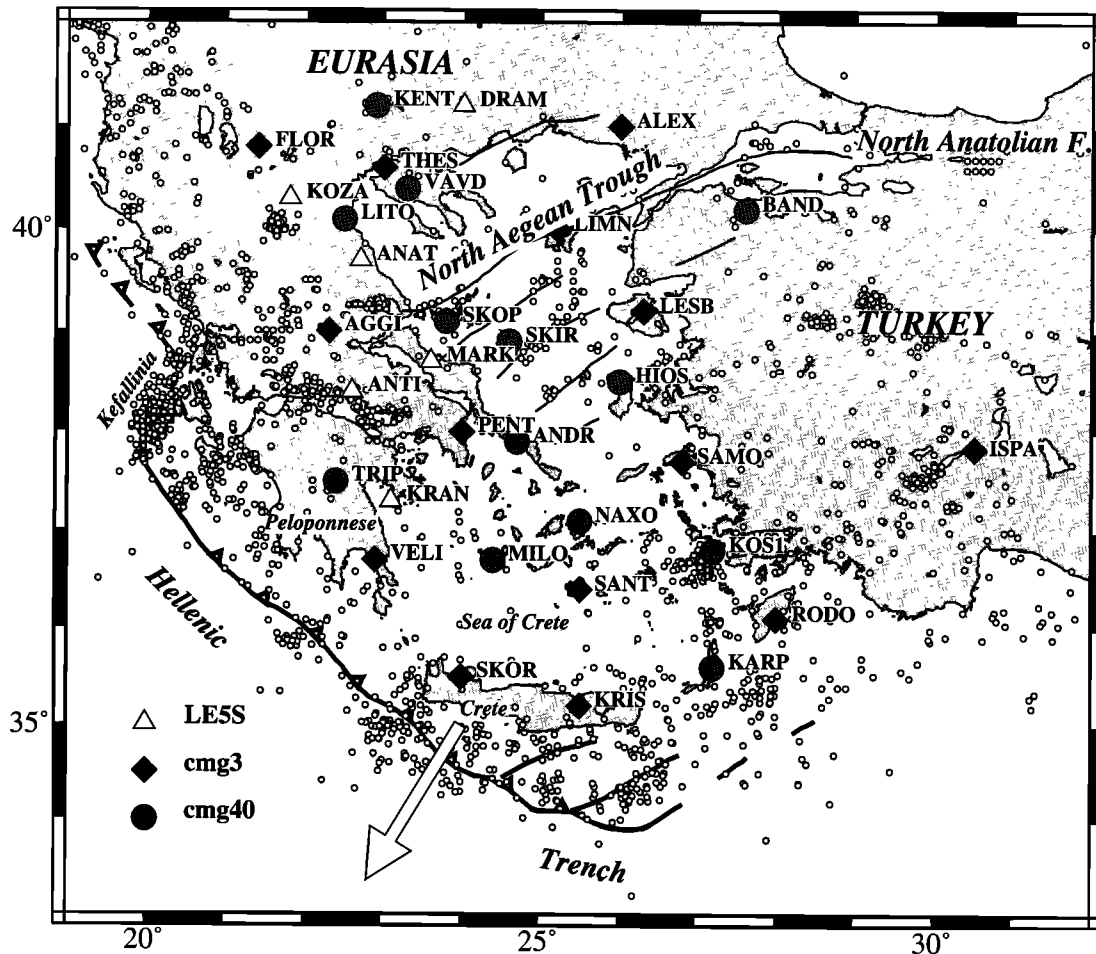


**Figure 1.** General sketch of the Aegean showing the main active boundaries and the seismological stations which were used for the anisotropy study. The open dots are the National Earthquake Information Service (NEIS) earthquakes of magnitude  $>4.5$  located between 1963 and 1996. The white arrow is the motion of Aegean relative to Europe [Le Pichon *et al.*, 1995].

seismic and regional earthquakes (Figure 1). We installed stations both on Aegean islands (which did not allow a homogeneous distribution of stations over the Aegean region) and on continental Greece. The equipment consisted of Lennartz LE55 (5 s), Güralp CMG40 (20 or 60 s), and Güralp CMG3 (60 or 100 s) seismometers and Reftek 72A06 and Agecodagis TitanDat data loggers, which recorded continuously at a sample frequency of 50 or 62.5 samples per second, respectively. The time was synchronized by GPS receivers in all stations. Stations were installed in permanent observatories of the National Observatory of Athens, of the Seismological Network of Thessaloniki, and in temporary shelters, where the seismometers were protected from temperature variations. We visited all the stations every month to retrieve and check the data. Because of weather conditions, especially during the winter season, microseismic noise was very strong during some periods of time, and the signal-to-noise ratio was low. In total, we recorded  $\sim 180$  Gb of raw data.

During the period of the field experiment, National Earthquake Information Service (NEIS) located  $\sim 105$  earthquakes greater than magnitude 5.5 from which we extracted records from the raw data. Of those in the distance range  $85^{\circ}$ – $110^{\circ}$  suitable for SKS observations, only 11 events were greater than magnitude 6, and of those, only six provided reliable shear waves splitting estimates (Table 1). The back azimuths of the six

earthquakes are  $N15^{\circ}E$ ,  $N60^{\circ}E$ ,  $N75^{\circ}E$ ,  $N100^{\circ}E$ , and  $N260^{\circ}E$  and therefore are associated with different Fresnel zones [Alsina and Snieder, 1995].

We used the method described by Vinnik *et al.* [1989] and Farra *et al.* [1991] to compute anisotropy. Two examples are given in Figures 2a and 2b. We computed the displacement field by deconvolving the data with the instrument response. For the LE55 sensors, this means we broadened the frequency response up to  $\sim 20$  s over which useful signal could be retrieved. The LE55 results are consistent with the neighboring stations equipped with broadband sensors. The traces were then filtered (usually in the frequency band 10–50 s) to improve the signal-to-noise ratio, using a three-pole Butterworth filter when the microseismic noise due to the bad weather conditions was too high. In some cases we had to restrict the frequency band further because of the noise level. We identified the SKS phase on the seismogram and rotated the two horizontal components into the radial (R) and the transversal (T) components. When energy was clearly visible on the T component, we plotted the particle motion, which should be elliptical, thus helping to determine the time window for the analysis of the splitting. We computed the splitting parameters delay time  $\delta t$  and fast polarization direction  $\Phi$  by the grid search algorithm [Vinnik *et al.*, 1992], which minimizes the energy on the T component as a function of  $\delta t$  and  $\Phi$ .

Table 1. Earthquake Parameters

Number	Date	Time, UT	Latitude, °N	Longitude, °E	Magnitude	Depth, km	Back Azimuth	$\Delta$ , deg
1	March 11, 1997	1922:00	7.7	127.6	6.2	88	75	95
2	April 1, 1997	1842:14	-18.2	-69.3	5.8	113	260	105
3	April 23, 1997	1944:30	13.9	144.9	5.9	102	60	103
4	May 22, 1997	0750:55	18.7	-101.7	5.7	91	75	95
5	June 17, 1997	2103:40	51.3	-179.3	6.2	33	15	89
6	July 11, 1997	0955:12	-5.7	110.7	5.4	577	98	90
11	Nov. 12, 1996	1659:44	-15	-75.7	6.4	33	264	108
12	Nov. 21, 1996	0743:40	6.6	126.4	5.6	65	78	95
13	Dec. 31, 1996	1241:42	15.8	-93	5.3	100	189	103
14	Jan. 1, 1997	2232:32	-0.1	123.8	5.7	115	85	97
15	Jan. 17, 1997	1120:23	-8.9	123.5	6	120	93	102
16	Jan. 23, 1997	0215:23	-21.9	-65.6	6.2	275	255	108
17	July 20, 1997	1014:22	-23	-66.3	5.7	256	255	109
18	Sept. 2, 1997	1213:25	3.9	-75.7	6.2	222	283	100
19	Oct. 28, 1997	0615:19	-4.34	-76.7	6.5	130	277	106
20	Nov. 28, 1997	2253:42	-13.5	-68.8	6.3	587	265	105
21	Jan. 1, 1998	0611:22	24	142	6.4	92	58	91
22	April 1, 1998	2243:00	-39.8	-75.2	6.2	9	239	118
23	April 3, 1998	2201:50	-8	-74.8	6.2	165	268	102
24	April 20, 1998	2259:15	18.6	-101	5.9	67	311	108
25	May 13, 1998	2302:02	-5.1	151.7	6	33	71	122
26	May 21, 1998	0534:25	0.2	119.6	6.2	33	87	94
27	May 22-1998	0448:50	-17.7	-65.4	6	24	255	100
28	May 23-1998	1744:47	8.1	123.8	5.9	656	78	93
29	June 7, 1998	2320:13	16	-93.7	5.8	87	299	101
30	July 29, 1998	0714:24	-32.3	-71.3	6.3	52	249	118
31	Aug. 4, 1998	1859:18	-0.6	-80.4	6.2	19	278	101
32	Aug. 20, 1998	0640:54	28.9	139.4	6.1	422	52	157
33	Aug. 28, 1998	1240:57	-0.1	125.1	6.1	66	84	97
34	Aug. 30, 1998	0148:08	17	148.1	6.1	33	56	105
35	Sept. 2, 1998	0837:27	5.4	126.7	6.4	33	78	97
36	Sept. 3, 1998	1737:59	-29.3	-71.6	6.1	33	248	110
37	Sept. 21, 1998	0652:41	0.2	122.5	6.1	149	86	96
38	Sept. 28, 1998	1334:30	-8.2	112.5	6.3	153	98	92
39	Oct. 8, 1998	0451:43	-16	-71.5	6.1	136	261	105
40	Oct. 27, 1998	2116:21	2.9	128.6	5.9	63	80	99
41	Oct. 28, 1998	1625:03	0.8	125.9	6.2	33	83	98
42	Nov. 8, 1998	0725:50	-8.8	121.4	6.3	33	94	100
43	Nov. 29, 1998	1410:31	-2.1	124.9	6.5	33	86	99
44	Dec. 6, 1998	0047:14	1.3	126.2	6.3	33	83	98
45	Dec. 27, 1998	0038:26	-21.5	176.4	6.1	144	58	157
46	Jan. 12, 1999	0232:26	26.7	140.1	5.9	441	53	93
47	Jan. 28, 1999	0810:05	52.9	-169.1	6.3	67	8	91
48	March 4, 1999	0852:02	5.3	121.7	6.5	33	82	92
49	April 3, 1999	0617:13	-16.3	-72.3	6.4	33	261	106
50	June 2, 1999	0023:19	0.1	123.5	5.8	161	85	97
51	June 15, 1999	2042:06	18.4	-97.4	6.5	71	305	104
52	June 18, 1999	1055:25	5.5	126.7	6.1	33	79	96
53	June 21, 1999	1743:04	18.3	-101.5	6	67	308	107
54	July 3, 1999	0530:10	26.3	140.4	6	433	55	93
55	Aug. 12, 1999	0544:58	-1.7	122.4	5.9	28	87	97
56	Aug. 20, 1999	1002:22	9.2	-84.1	6	33	289	10

The reliability of the result is estimated in three ways: (1) from the visual fit of the theoretical T component seismogram calculated with the estimated splitting parameters from the observed R component, (2) from the energy reduction on T after correction for splitting, which should be >50%, and (3) from the signal-to-noise ratio of the SKS phase on R, which should be >3. We assigned a quality factor to each measurement of either good or fair that depended on the uncertainty both in  $\Phi$  and  $\delta t$ : good when errors in  $\Phi$  were <20° and those in  $\delta t$  were <0.3 s and fair when errors in  $\Phi$  were <45° and those in  $\delta t$  were <0.5 s. A low reduction value usually indicates small or null splitting and is considered reliable only if the signal-to-noise ratio is >5 on the R component. Then, for each

station, we computed a weighted average (depending on the respective uncertainties in  $\delta t$  and in  $\Phi$ ) of the individual nonnull values.

### 3. Results

The results consist of two parameters: the time delay  $\delta t$  and the polarization direction  $\Phi$  of the faster of the two quasi-S waves (Table 2 and Figure 3). In total, we estimated 150 splitting parameters from data of six earthquakes. We complemented these results with SKS splitting measurements (Table 3) for records obtained from temporary GEOFON stations in the

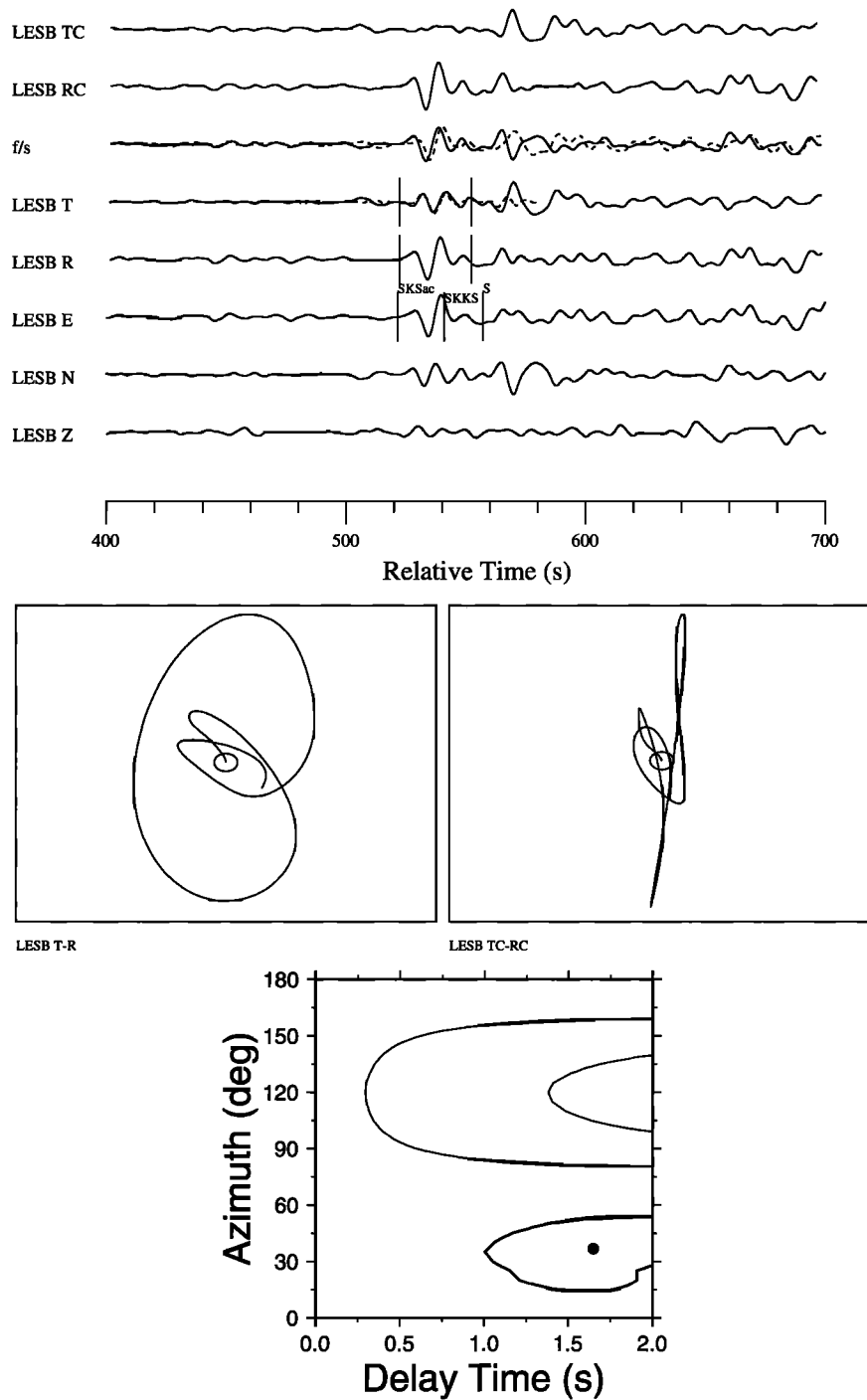


**Figure 2a.** Example of shear wave splitting for the event on March 11, 1997, in station LESB located in Lesbos. The top panel shows band-pass filtered (0.02–0.1 Hz) seismograms. The horizontal N and E components were rotated into the R and T components. Superimposed (dashed line) on the T component is a theoretical T seismogram obtained from the R component assuming  $\Phi = N37^\circ E$  and  $\delta t = 1.65$  s. The window for the splitting analysis is marked by vertical bars on the R and T components. The traces marked f/s show the horizontal seismograms rotated into the direction of the faster and slower quasi-S waves. The top traces marked RC and TC are the R and T component seismograms corrected for splitting effect. The middle panels show polarization diagrams of the SKS window (left) before and (right) after removal of the splitting effect. The bottom panel shows a contour diagram of the energy on the T component as a function of the splitting parameters  $\delta t$  and  $\Phi$ . Contours are plotted as multiples of the 95% significance level indicated by the thick line and calculated after *Silver and Chan* [1991].

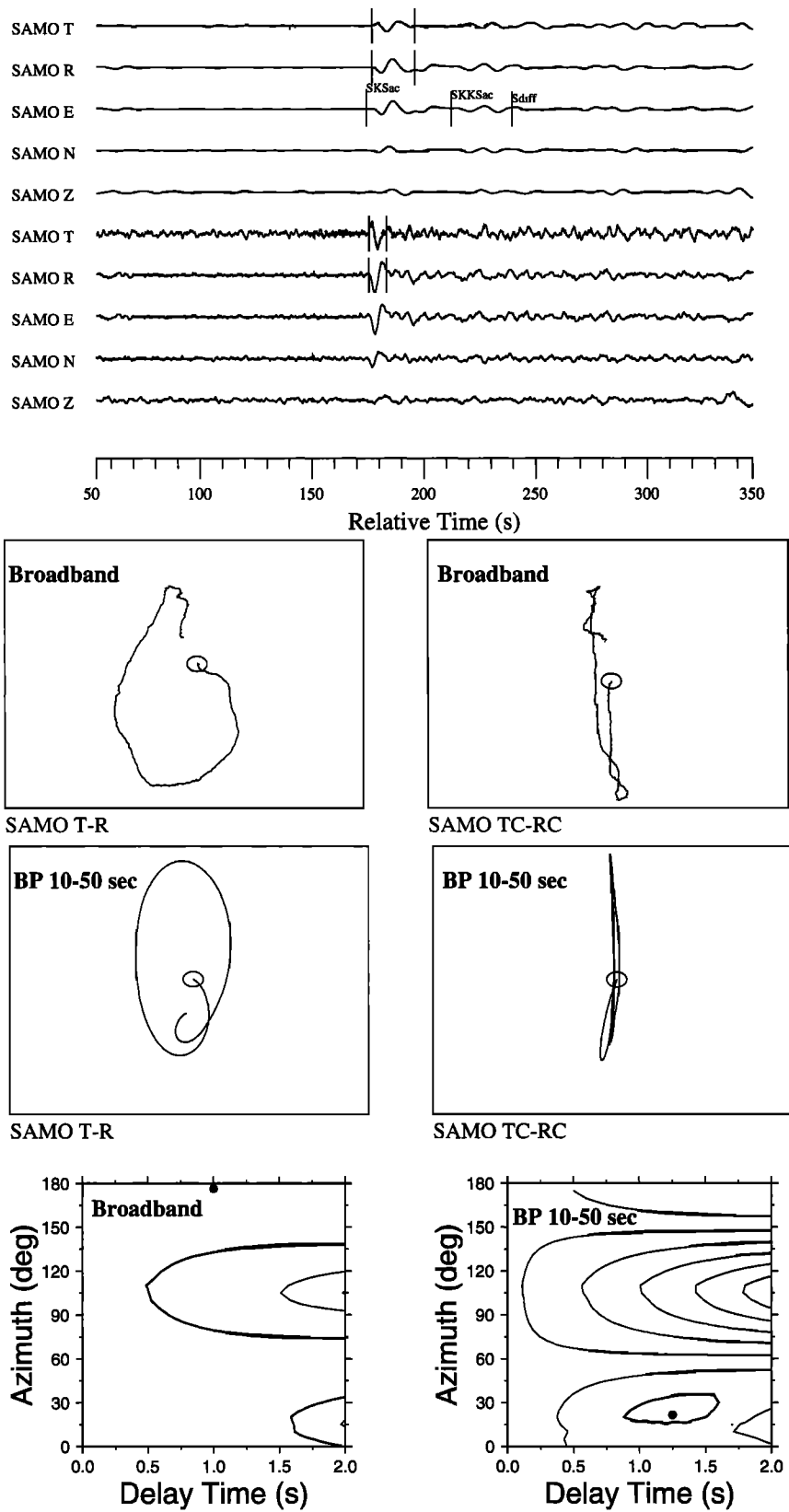


**Figure 2b.** Example of shear wave splitting for the event on April 23, 1997, in station SAMO located in Samos. The top panel shows raw broadband data and band-pass filtered (0.02–0.1 Hz) seismograms. In the middle panels the polarization diagrams are computed for both the broadband and filtered data. In the bottom panels we note that the 95% error bounds are much wider for broadband data than for filtered data. Generally, the microseismic noise was high because of bad weather conditions and filtering was necessary.

**Table 2.** Anisotropy Parameters Obtained During the Aegean Experiment

Station	$\Phi^a$	$\sigma\Phi^b$	$\delta^c$	$\sigma\delta^d$	mpf <sup>e</sup>	Filters <sup>f</sup>	Remark	Event
AGGI	39	17	0.4	0.3	41	10–50	good	1
AGGI <sup>g</sup>	176 <sup>g</sup>	45 <sup>g</sup>	0.1 <sup>g</sup>	0.5 <sup>g</sup>	99 <sup>g</sup>	10–50 <sup>g</sup>	good null <sup>g</sup>	2 <sup>g</sup>
AGGI	27	16	0.6	0.2	40	raw	good	3
AGGI	16	20	0.3	0.2	43	>3	good	4
AGGI <sup>g</sup>	90 <sup>g</sup>	45 <sup>g</sup>	0.5 <sup>g</sup>	0.5 <sup>g</sup>	97 <sup>g</sup>	>2 <sup>g</sup>	fair null <sup>g</sup>	5 <sup>g</sup>
AGGI <sup>g</sup>	83 <sup>g</sup>	45 <sup>g</sup>	0.05 <sup>g</sup>	0.5 <sup>g</sup>	99 <sup>g</sup>	10–50 <sup>g</sup>	good null <sup>g</sup>	6 <sup>g</sup>
AGGI <sup>h</sup>	28 <sup>h</sup>	10 <sup>h</sup>	0.44 <sup>h</sup>	0.13 <sup>h</sup>				
ALEX	1	45	1.05	0.5	55	raw	fair	1
ALEX	4	45	1.55	0.5	72	>3	fair	2
ALEX	0	45	1.8	0.5	43	>3	fair	3
ALEX	24	45	1.3	0.5	70	>3	fair	4
ALEX	42	16	0.4	0.2	34	3–20	good	6
ALEX <sup>h</sup>	30 <sup>h</sup>	13 <sup>h</sup>	0.8 <sup>h</sup>	0.15 <sup>h</sup>				
ANAT	134	20	0.65	0.5	59	3–20	fair	1
ANAT <sup>g</sup>	142 <sup>g</sup>	45 <sup>g</sup>	0.9 <sup>g</sup>	0.5 <sup>g</sup>	92 <sup>g</sup>	raw <sup>g</sup>	good null <sup>g</sup>	3 <sup>g</sup>
ANAT	156	45	0.85	0.5	70	>2	fair	4
ANAT <sup>g</sup>	108 <sup>g</sup>	45 <sup>g</sup>	1.3 <sup>g</sup>	0.5 <sup>g</sup>	91 <sup>g</sup>	>2 <sup>g</sup>	fair null <sup>g</sup>	5 <sup>g</sup>
ANAT <sup>g</sup>	145 <sup>g</sup>	45 <sup>g</sup>	0.25 <sup>g</sup>	0.5 <sup>g</sup>	80 <sup>g</sup>	>2 <sup>g</sup>	fair null <sup>g</sup>	6 <sup>g</sup>
ANAT <sup>h</sup>	137 <sup>h</sup>	18 <sup>h</sup>	0.75 <sup>h</sup>	0.35 <sup>h</sup>				
ANDR <sup>g</sup>	90 <sup>g</sup>	45 <sup>g</sup>	0.95 <sup>g</sup>	0.5 <sup>g</sup>	77 <sup>g</sup>	>3 <sup>g</sup>	fair null <sup>g</sup>	5 <sup>g</sup>
ANDR <sup>g</sup>	11 <sup>g</sup>	45 <sup>g</sup>	0.35 <sup>g</sup>	0.5 <sup>g</sup>	99 <sup>g</sup>	>2 <sup>g</sup>	good null <sup>g</sup>	6 <sup>g</sup>
BAND <sup>h</sup>	21 <sup>h</sup>	45 <sup>h</sup>	1.1 <sup>h</sup>	0.5 <sup>h</sup>	46 <sup>h</sup>	>5 <sup>h</sup>	good <sup>h</sup>	3 <sup>h</sup>
HIOS	37	45	0.8	0.5	65	10–50	fair	1
HIOS	58	45	1.35	0.5	76	10–50	fair	2
HIOS	26	45	1.85	0.5	37	10–50	fair	3
HIOS <sup>g</sup>	29 <sup>g</sup>	45 <sup>g</sup>	1.15 <sup>g</sup>	0.5 <sup>g</sup>	87 <sup>g</sup>	>3 <sup>g</sup>	good null <sup>g</sup>	4 <sup>g</sup>
HIOS <sup>g</sup>	20 <sup>g</sup>	45 <sup>g</sup>	0.95 <sup>g</sup>	0.5 <sup>g</sup>	99 <sup>g</sup>	10–50 <sup>g</sup>	fair null <sup>g</sup>	5 <sup>g</sup>
HIOS <sup>g</sup>	102 <sup>g</sup>	45 <sup>g</sup>	1.1 <sup>g</sup>	0.5 <sup>g</sup>	94 <sup>g</sup>	3–20 <sup>g</sup>	good null <sup>g</sup>	6 <sup>g</sup>
HIOS <sup>h</sup>	40 <sup>h</sup>	26 <sup>h</sup>	1.33 <sup>h</sup>	0.29 <sup>h</sup>				
DRAM <sup>h</sup>	40 <sup>h</sup>	17 <sup>h</sup>	0.6 <sup>h</sup>	0.3 <sup>h</sup>	45 <sup>h</sup>	10–20 <sup>h</sup>	good <sup>h</sup>	1 <sup>h</sup>
FLOR <sup>g</sup>	99 <sup>g</sup>	45 <sup>g</sup>	0.15 <sup>g</sup>	0.5 <sup>g</sup>	82 <sup>g</sup>	10–50 <sup>g</sup>	good null <sup>g</sup>	1 <sup>g</sup>
FLOR <sup>g</sup>	157 <sup>g</sup>	45 <sup>g</sup>	0.85 <sup>g</sup>	0.5 <sup>g</sup>	86 <sup>g</sup>	>3 <sup>g</sup>	good null <sup>g</sup>	2 <sup>g</sup>
FLOR	22	20	0.4	0.5	50	10–50	fair	3
FLOR	145	45	0.55	0.5	40	>2	fair	4
FLOR	177	20	1.35	0.5	58	>2	fair	5
FLOR	130	12	0.45	0.1	41	3–20	good	6
FLOR <sup>h</sup>	154 <sup>h</sup>	9 <sup>h</sup>	0.48 <sup>h</sup>	0.09 <sup>h</sup>				
KARP	2	45	0.7	0.5	57	10–50	fair	1
KARP <sup>g</sup>	163 <sup>g</sup>	45 <sup>g</sup>	0.5 <sup>g</sup>	0.5 <sup>g</sup>	99 <sup>g</sup>	10–50 <sup>g</sup>	fair null <sup>g</sup>	2 <sup>g</sup>
KARP	177	45	0.8	0.5	64	raw	fair	3
KARP	24	16	1.15	0.4	52	>3	fair	4
KARP <sup>g</sup>	36 <sup>g</sup>	45 <sup>g</sup>	0.5 <sup>g</sup>	0.5 <sup>g</sup>	85 <sup>g</sup>	10–50 <sup>g</sup>	good null <sup>g</sup>	5 <sup>g</sup>
KARP	38	45	0.25	0.5	45	>2	fair	6
KARP <sup>h</sup>	21 <sup>h</sup>	14 <sup>h</sup>	0.77 <sup>h</sup>	0.23 <sup>h</sup>				
KENT <sup>g</sup>	180 <sup>g</sup>	45 <sup>g</sup>	1 <sup>g</sup>	0.5 <sup>g</sup>	65 <sup>g</sup>	10–50 <sup>g</sup>	fair null <sup>g</sup>	1 <sup>g</sup>
KENT <sup>g</sup>	157 <sup>g</sup>	45 <sup>g</sup>	0.3 <sup>g</sup>	0.5 <sup>g</sup>	75 <sup>g</sup>	<10 <sup>g</sup>	fair null <sup>g</sup>	4 <sup>g</sup>
KOS1	43	15	0.65	0.2	32	10–50	good	1
KOS1 <sup>g</sup>	174 <sup>g</sup>	45 <sup>g</sup>	2.7 <sup>g</sup>	0.5 <sup>g</sup>	97 <sup>g</sup>	10–50 <sup>g</sup>	fair null <sup>g</sup>	2 <sup>g</sup>
KOS1	154	45	0.75	0.5	48	>3	fair	4
KOS1 <sup>h</sup>	54 <sup>h</sup>	14 <sup>h</sup>	0.66 <sup>h</sup>	0.18 <sup>h</sup>				
KOZA <sup>g</sup>	79 <sup>g</sup>	45 <sup>g</sup>	1.1 <sup>g</sup>	0.5 <sup>g</sup>	88 <sup>g</sup>	3–20 <sup>g</sup>	fair null <sup>g</sup>	1 <sup>g</sup>
KOZA	156	10	0.75	0.25	38	>3	good	4
KOZA	160	45	0.4	0.5	74	2–10	fair	6
KOZA <sup>h</sup>	156 <sup>h</sup>	10 <sup>h</sup>	0.68 <sup>h</sup>	0.22 <sup>h</sup>				
LESB	37	15	1.65	0.3	41	10–50	good	1
LESB <sup>g</sup>	125 <sup>g</sup>	45 <sup>g</sup>	0.6 <sup>g</sup>	0.5 <sup>g</sup>	95 <sup>g</sup>	>3 <sup>g</sup>	good null <sup>g</sup>	4 <sup>g</sup>
LESB	45	7.5	1.55	0.3	43	10–50	good	5
LESB	12	45	1.25	0.5	79	>3	fair	6
LESB <sup>h</sup>	42 <sup>h</sup>	6 <sup>h</sup>	1.5 <sup>h</sup>	0.18 <sup>h</sup>				
LIMN	11	45	2	0.7	53	10–50	fair	1
LIMN	49	20	1.1	0.4	58	10–50	fair	2
LIMN	25	45	2.2	0.7	44	10–50	fair	3
LIMN	18	45	0.9	0.5	74	>3	fair	4
LIMN	35	16	1.2	0.5	59	10–50	good	5
LIMN <sup>g</sup>	257 <sup>g</sup>	45 <sup>g</sup>	0.35 <sup>g</sup>	0.5 <sup>g</sup>	77 <sup>g</sup>	3–20 <sup>g</sup>	fair null <sup>g</sup>	6 <sup>g</sup>
LIMN <sup>h</sup>	36 <sup>h</sup>	11 <sup>h</sup>	1.3 <sup>h</sup>	0.23 <sup>h</sup>				
LITO <sup>g</sup>	150 <sup>g</sup>	45 <sup>v</sup>	1.45 <sup>g</sup>	0.5 <sup>g</sup>	76 <sup>g</sup>	10–50 <sup>g</sup>	fair null <sup>g</sup>	1 <sup>g</sup>
LITO <sup>g</sup>	152 <sup>g</sup>	45 <sup>g</sup>	2.8 <sup>g</sup>	0.7 <sup>v</sup>	91 <sup>g</sup>	10–50 <sup>g</sup>	fair null <sup>g</sup>	2 <sup>g</sup>
LITO <sup>g</sup>	137 <sup>g</sup>	45 <sup>g</sup>	1.3 <sup>v</sup>	0.5 <sup>g</sup>	88 <sup>g</sup>	10–20 <sup>g</sup>	fair null <sup>g</sup>	3 <sup>g</sup>
LITO <sup>g</sup>	136 <sup>g</sup>	45 <sup>g</sup>	0.45 <sup>g</sup>	0.5 <sup>g</sup>	90 <sup>g</sup>	>3 <sup>g</sup>	good null <sup>g</sup>	4 <sup>g</sup>
MILO	11	20	0.55	0.45	45	10–20	good	1
MILO <sup>g</sup>	72 <sup>g</sup>	45 <sup>g</sup>	0.4 <sup>g</sup>	0.5 <sup>g</sup>	99 <sup>g</sup>	10–20 <sup>g</sup>	good null <sup>g</sup>	2 <sup>g</sup>
MILO	170	17	0.55	0.4	53	5–50	fair	3

Table 2. (continued)

Station	$\Phi^a$	$\sigma\Phi^b$	$\delta^c$	$\sigma\delta^d$	mpf <sup>e</sup>	Filters <sup>f</sup>	Remark	Event
MILO <sup>g</sup>	17 <sup>g</sup>	20 <sup>g</sup>	1.05 <sup>g</sup>	0.5 <sup>g</sup>	50 <sup>g</sup>	>3 <sup>g</sup>	fair null <sup>g</sup>	4 <sup>g</sup>
MILO <sup>g</sup>	114 <sup>g</sup>	45 <sup>g</sup>	0.3 <sup>g</sup>	0.5 <sup>g</sup>	92 <sup>g</sup>	10–50 <sup>g</sup>	good null <sup>g</sup>	5 <sup>g</sup>
MILO	141	45	0.55	0.5	36	>2	fair	6
MILO <sup>h</sup>	175 <sup>h</sup>	12 <sup>h</sup>	0.55 <sup>h</sup>	0.25 <sup>h</sup>				
NAXO	2	45	0.8	0.5	80	10–50	fair	1
NAXO	53	45	0.45	0.7	72	10–50	fair	2
NAXO	23	45	0.8	0.5	63	>3	fair	4
NAXO <sup>g</sup>	25 <sup>g</sup>	45 <sup>g</sup>	1.3 <sup>g</sup>	0.5 <sup>g</sup>	80 <sup>g</sup>	10–50 <sup>g</sup>	fair null <sup>g</sup>	5 <sup>g</sup>
NAXO	42	45	0.25	0.5	41	>2	fair	6
NAXO <sup>h</sup>	30 <sup>h</sup>	22 <sup>h</sup>	0.6 <sup>h</sup>	0.26 <sup>h</sup>				
PENT <sup>g</sup>	95 <sup>g</sup>	45 <sup>g</sup>	0.3 <sup>g</sup>	0.5 <sup>g</sup>	77 <sup>g</sup>	10–50 <sup>g</sup>	good null <sup>g</sup>	1 <sup>g</sup>
PENT <sup>g</sup>	172 <sup>g</sup>	45 <sup>g</sup>	0.65 <sup>g</sup>	0.5 <sup>g</sup>	98 <sup>g</sup>	10–50 <sup>g</sup>	good null <sup>g</sup>	2 <sup>g</sup>
PENT <sup>g</sup>	54 <sup>g</sup>	20 <sup>g</sup>	1.6 <sup>g</sup>	0.5 <sup>g</sup>	75 <sup>g</sup>	10–50 <sup>g</sup>	good null <sup>g</sup>	3 <sup>g</sup>
PENT <sup>g</sup>	180 <sup>g</sup>	45 <sup>g</sup>	0.15 <sup>g</sup>	0.5 <sup>g</sup>	97 <sup>g</sup>	10–50 <sup>g</sup>	good null <sup>g</sup>	5 <sup>g</sup>
PENT <sup>g</sup>	161 <sup>g</sup>	45 <sup>g</sup>	0.1 <sup>g</sup>	0.5 <sup>g</sup>	90 <sup>g</sup>	>2 <sup>g</sup>	good null <sup>g</sup>	6 <sup>g</sup>
RODO	49	11	1.1	0.2	35	10–50	good	2
RODO	177	45	1.5	0.5	50	10–50	fair	3
RODO <sup>g</sup>	35 <sup>g</sup>	54 <sup>g</sup>	1.35 <sup>g</sup>	0.5 <sup>g</sup>	75 <sup>g</sup>	>3 <sup>g</sup>	fair null <sup>g</sup>	4 <sup>g</sup>
RODO <sup>g</sup>	110 <sup>g</sup>	45 <sup>g</sup>	1.4 <sup>g</sup>	0.5 <sup>g</sup>	91 <sup>g</sup>	10–50 <sup>g</sup>	good null <sup>g</sup>	5 <sup>g</sup>
RODO <sup>h</sup>	46 <sup>h</sup>	10 <sup>h</sup>	1.15 <sup>h</sup>	0.18 <sup>h</sup>				
SAMO	52	18	0.55	0.4	34	10–50	fair	1
SAMO <sup>g</sup>	179 <sup>g</sup>	45 <sup>g</sup>	0.75 <sup>g</sup>	0.5 <sup>g</sup>	83 <sup>g</sup>	10–50 <sup>g</sup>	good null <sup>g</sup>	2 <sup>g</sup>
SAMO	21	2	1.2	0.1	23	10–50	good	3
SAMO	15	45	1.35	0.5	48	>3	fair	4
SAMO	175	45	0.95	0.5	48	10–50	fair	5
SAMO <sup>g</sup>	93 <sup>g</sup>	45 <sup>g</sup>	1.05 <sup>g</sup>	0.5 <sup>g</sup>	92 <sup>g</sup>	>2 <sup>g</sup>	good null <sup>g</sup>	6 <sup>g</sup>
SAMO <sup>h</sup>	21 <sup>h</sup>	2 <sup>h</sup>	1.15 <sup>h</sup>	0.09 <sup>h</sup>				
SKIR	41	15	2.4	0.6	35	10–20	fair	1
SKIR <sup>g</sup>	117 <sup>g</sup>	45 <sup>g</sup>	2 <sup>g</sup>	0.5 <sup>g</sup>	93 <sup>g</sup>	>3 <sup>g</sup>	fair null <sup>g</sup>	4 <sup>g</sup>
SKIR <sup>h</sup>	41 <sup>h</sup>	15 <sup>h</sup>	2.4 <sup>h</sup>	0.6 <sup>h</sup>				
SKOP <sup>g</sup>	69 <sup>g</sup>	45 <sup>g</sup>	0.3 <sup>g</sup>	0.8 <sup>g</sup>	85 <sup>g</sup>	10–20 <sup>g</sup>	good null <sup>g</sup>	1 <sup>g</sup>
SKOP <sup>g</sup>	163 <sup>g</sup>	45 <sup>g</sup>	0.8 <sup>g</sup>	0.5 <sup>g</sup>	93 <sup>g</sup>	5–30 <sup>g</sup>	fair null <sup>g</sup>	3 <sup>g</sup>
SKOP <sup>g</sup>	17 <sup>g</sup>	45 <sup>g</sup>	0.4 <sup>g</sup>	0.5 <sup>g</sup>	77 <sup>g</sup>	>3 <sup>g</sup>	fair null <sup>g</sup>	4 <sup>g</sup>
THES <sup>g</sup>	59 <sup>g</sup>	45 <sup>g</sup>	0.35 <sup>g</sup>	0.5 <sup>g</sup>	95 <sup>g</sup>	raw <sup>g</sup>	good null <sup>g</sup>	1 <sup>g</sup>
THES	107	45	0.6	0.5	44	raw	fair	4
THES <sup>g</sup>	120 <sup>g</sup>	20 <sup>g</sup>	0.1 <sup>g</sup>	0.2 <sup>g</sup>	67 <sup>g</sup>	raw <sup>g</sup>	fair null <sup>g</sup>	6 <sup>g</sup>
THES <sup>h</sup>	107 <sup>h</sup>	45 <sup>h</sup>	0.6 <sup>h</sup>	0.5 <sup>h</sup>				
TRIP <sup>g</sup>	175 <sup>g</sup>	45 <sup>g</sup>	1.3 <sup>g</sup>	0.5 <sup>g</sup>	79 <sup>g</sup>	>3 <sup>g</sup>	good null <sup>g</sup>	1 <sup>g</sup>
TRIP	168	45	1.15	0.5	70	10–50	fair	3
TRIP <sup>g</sup>	140 <sup>g</sup>	45 <sup>g</sup>	0.3 <sup>g</sup>	0.5 <sup>g</sup>	50 <sup>g</sup>	>3 <sup>g</sup>	fair null <sup>g</sup>	4 <sup>g</sup>
TRIP <sup>h</sup>	168 <sup>h</sup>	45 <sup>h</sup>	1.15 <sup>h</sup>	0.5 <sup>h</sup>				
VAVD <sup>g</sup>	79 <sup>g</sup>	45 <sup>g</sup>	1.5 <sup>g</sup>	0.5 <sup>g</sup>	79 <sup>g</sup>	>3 <sup>g</sup>	fair null <sup>g</sup>	1 <sup>g</sup>
VELI	131	45	0.55	0.5	69	3–50	fair	2
VELI	158	16	1.75	0.4	53	10–50	fair	3
VELI	156	17	0.75	0.3	40	>3	good	4
VELI	168	17	1.1	0.4	40	Raw	good	5
VELI	170	20	2.55	0.7	53	10–50	fair	6
VELI <sup>h</sup>	161 <sup>h</sup>	9 <sup>h</sup>	1.13 <sup>h</sup>	0.18 <sup>h</sup>				

<sup>a</sup>Orientation of the fast splitting direction.<sup>b</sup>Associated error in degree of orientation of the fast splitting direction.<sup>c</sup>Delay time between the two quasi-S waves.<sup>d</sup>Associated error of the delay time (in seconds).<sup>e</sup>Minimum penalty function [Farra *et al.*, 1991].<sup>f</sup>Filters give the signal band pass in seconds.<sup>g</sup>Null measurements, which are not used for the calculation of the average.<sup>h</sup>Weighted averages (including only nonnull values) with associated uncertainties reported for each station.

islands of Crete and Santorini (SKOR, KRIS, and SANT in Figure 1) and data recorded at the permanent GEOFON station of Isparta (ISPA, Turkey). The operating period for the latter three stations is longer compared to the stations we operated. Most of the splitting parameters were computed for the broadband data over a wide frequency band, but because of microseismic noise around 7 s, we had to narrow the frequency band for some records in order to improve the signal-to-noise ratio.

Observed splitting parameters are not homogenous over the Aegean. However, values of  $\Phi$ , although scattered in some stations, are not linked to back azimuth (on an average 15°, 60°, 75°, 98°, and 260°). This suggests that the observed

splitting parameters are unlikely to be caused by varying anisotropy within different layers. Back azimuths vary by only  $\pm 2^\circ$  over the entire seismological network, which according to our reading uncertainties, is too small to be used for a study of azimuthal dependence of  $\Phi$  for different stations. Relatively large delay times are observed beneath most of the islands of the northern Aegean Sea and in western Turkey. Values as large as 2 s are observed in stations ALEX, BAND, LIMN, LESB, SKIR, HIOS, and SAMO. At some stations (BAND and SKIR) we have only one measurement, but their values are consistent with these at neighboring stations. No clear splitting was observed at SKOP. This station was generally noisy and reliable splitting analysis could be carried out only

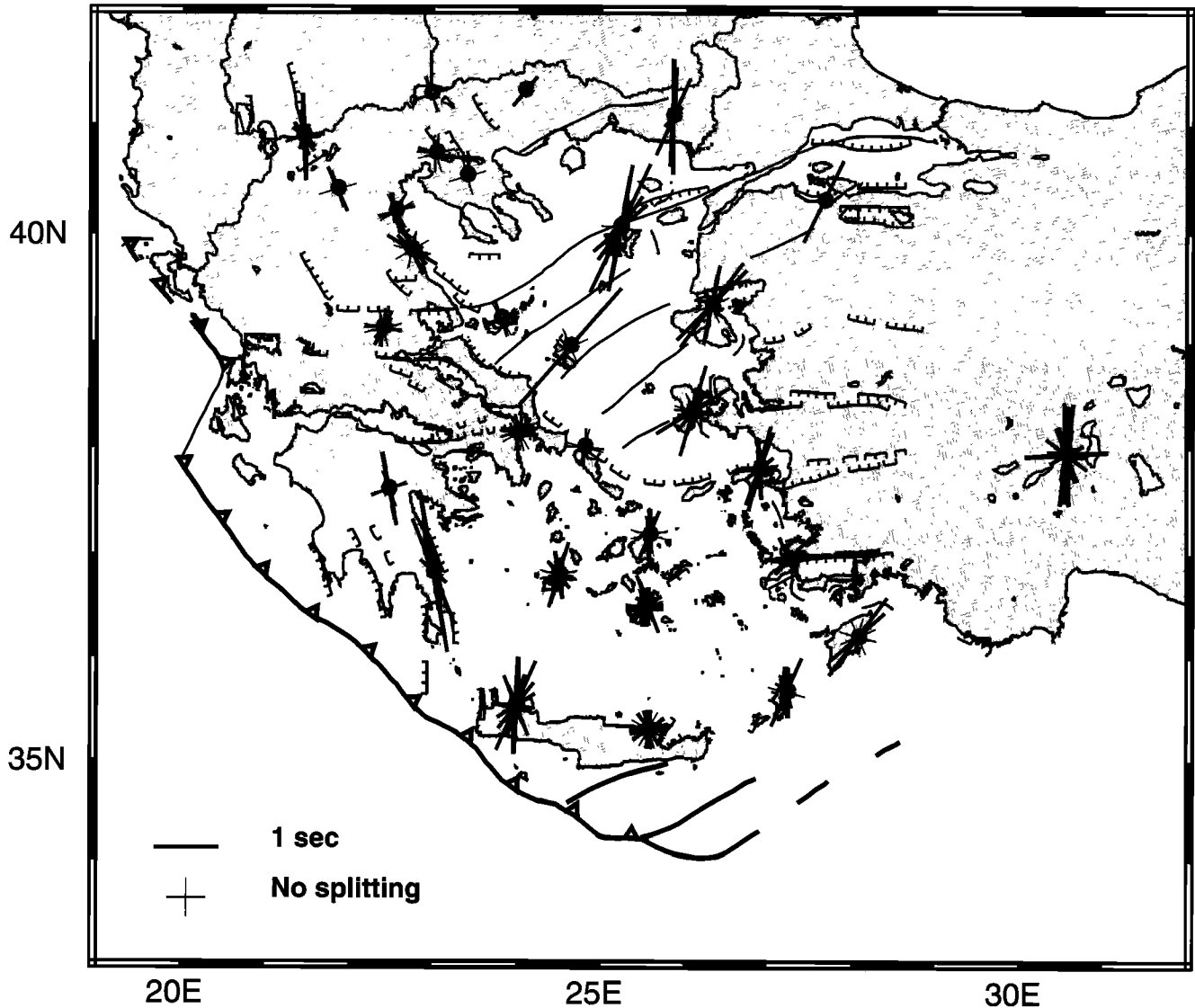


**Figure 3.** Map of the fast polarization direction of anisotropy superimposed on the active faults of the Aegean. We report all individual measurements (thick lines) in all stations. Null measurements are depicted with a cross oriented on the back azimuth and at  $90^\circ$ . There is no clear alignment of  $\Phi$  with the most important strike-slip faults at the western termination of the north Anatolian fault into the north Aegean Sea.

for the event of May 22, 1997, which was well recorded and clearly shows no anisotropy.

In contrast, the stations located in continental Greece (e.g., AGGI, ANAT, DRAM, FLOR, KOZA, and THES) show small delay times ( $<0.8$  s) or, in some cases, null values (KENT, LITO, PENT, and VAVD). This is also the case beneath the Sea of Crete (e.g., ANDR, NAXO, MILO, SANT, and KOS1) and Crete (SKOR and KRIS). Delay times  $>1$  s are observed only at TRIP and VELI. For station VELI in southern Peloponnese we observe a mean delay of 1.1 s, which is greater than those at neighboring stations but well constrained and consistent in orientation with the observations at TRIP.

The fast polarization direction  $\Phi$  is not homogenous over the Aegean (Figure 3). In the northern Aegean Sea, and especially in the northeast,  $\Phi$  varies between  $N10^\circ$  and  $N50^\circ E$  (e.g., AGGI, HIOS, KOS1, LESB, LIMN, SAMO, and SKIR). In continental Greece,  $\Phi$  varies between  $N150^\circ$  and  $N180^\circ E$  and is significantly different from the stations in the Aegean Sea. Beneath the stations of KARP and RODO, in the eastern Hellenic arc,  $\Phi$  is between  $N20^\circ$  and  $N50^\circ E$ .

In summary, we note that the observed anisotropy is not homogenous over the Aegean region, either in terms of time delays or fast polarization directions. There is not a random scatter, but we observe some regional consistency between the observations. The most coherent and large time delays ( $>1$  s) are seen in the north Aegean Sea, where a consistent orientation trending approximately  $N20^\circ E$  is found. Small delay times or null results are observed in the Sea of Crete and in Continental Greece. The fast polarization direction trends roughly NNE-SSW in the eastern part and NNW-SSE in the western part, i.e., parallel to the Hellenic arc.

Because anisotropy is generally attributed to upper mantle flow in oceanic regions or to lithospheric (present or frozen) deformation in continental regions we will compare our results with other measurements in the Aegean that are related to geological processes and to deformation. In order to smooth the observations we compute a weighted average (depending on the respective uncertainties) both of the delay times and of the fast polarization direction for each station (Tables 2 and 3). Because the Aegean is a region of intense and heterogeneous

**Table 3.** Anisotropy Results Obtained for Miscellaneous Stations in the Aegean Area

Station	$\Phi^a$	$\delta^b$	Filters <sup>c</sup>	Remark	Event
ISPA <sup>d</sup>			raw <sup>d</sup>	good null <sup>d</sup>	97-01-23 <sup>d</sup>
ISPA	2	1.5	raw	good	97-05-22
ISPA	8	1.6	raw	fair	97-06-17
ISPA <sup>d</sup>			10-50 <sup>d</sup>	fair null <sup>d</sup>	97-07-20 <sup>d</sup>
ISPA	158	0.9	10-50	very good	97-09-02
ISPA	127	0.8	raw	good	97-10-28
ISPA	115	0.35	raw	good	97-11-28
ISPA	13	0.8	raw	good	98-01-01
ISPA	128	0.65	raw	very good	98-04-03
ISPA	177	1.6	10-50	very good	98-04-20
ISPA	98	0.6	raw	fair	98-05-22
ISPA	179	1.1	10-50	fair	98-07-29
ISPA	163	0.9	raw	good	98-08-04
ISPA	61	0.6	>2	good	98-09-02
ISPA <sup>d</sup>			raw <sup>d</sup>	good null <sup>d</sup>	98-10-08 <sup>d</sup>
ISPA	86	1.3	raw	fair	98-11-08
ISPA <sup>c</sup>	177 ± 13	1.7 ± 0.35 <sup>e</sup>			
ISPA <sup>c</sup>	102 ± 26	0.7 ± 0.3 <sup>c</sup>			
KRIS <sup>d</sup>	89 <sup>d</sup>	1.15 <sup>d</sup>	raw <sup>d</sup>	good null <sup>d</sup>	96-11-12 <sup>d</sup>
KRIS <sup>d</sup>	59 <sup>d</sup>	0.25 <sup>d</sup>	raw <sup>d</sup>	good null <sup>d</sup>	96-11-21 <sup>d</sup>
KRIS <sup>d</sup>	130 <sup>d</sup>	0.45 <sup>d</sup>	raw <sup>d</sup>	good null <sup>d</sup>	96-12-31 <sup>d</sup>
KRIS <sup>d</sup>	0 <sup>d</sup>	0.65 <sup>d</sup>	raw <sup>d</sup>	good null <sup>d</sup>	97-01-01 <sup>d</sup>
KRIS <sup>d</sup>	87 <sup>d</sup>	1.25 <sup>d</sup>	raw <sup>d</sup>	good null <sup>d</sup>	97-01-17 <sup>d</sup>
KRIS <sup>d</sup>	137 <sup>d</sup>	0.25 <sup>d</sup>	raw <sup>d</sup>	good null <sup>d</sup>	97-01-23 <sup>d</sup>
KRIS <sup>d</sup>	82 <sup>d</sup>	0.9 <sup>d</sup>	raw <sup>d</sup>	good null <sup>d</sup>	97-03-11 <sup>d</sup>
SANT	2	0.4	raw	good	97-07-20
SANT <sup>d</sup>			raw <sup>d</sup>	good null <sup>d</sup>	98-04-03 <sup>d</sup>
SANT <sup>d</sup>			raw <sup>d</sup>	good null <sup>d</sup>	98-05-21 <sup>d</sup>
SANT	61	0.5	3-20	fair	98-05-13
SANT <sup>d</sup>			raw <sup>d</sup>	good null <sup>d</sup>	98-05-23 <sup>d</sup>
SANT <sup>d</sup>			10-50 <sup>d</sup>	fair null <sup>d</sup>	98-08-04 <sup>d</sup>
SANT	178	0.5	3-20	good	98-08-20
SANT <sup>d</sup>			3-50 <sup>d</sup>	fair null <sup>d</sup>	98-08-28
SANT	4	0.5	3-20	good	98-09-02
SANT	118	0.4	3-20	good	98-09-28
SANT <sup>d</sup>			3-20 <sup>d</sup>	fair null <sup>d</sup>	98-11-08 <sup>d</sup>
SANT	56	0.3	raw	good	98-11-29
SANT	29	0.5	raw	good	98-01-28
SANT <sup>d</sup>			3-50 <sup>d</sup>	good null <sup>d</sup>	99-03-04 <sup>d</sup>
SANT <sup>d</sup>			3-20 <sup>d</sup>	good null <sup>d</sup>	99-04-03 <sup>d</sup>
SANT <sup>c</sup>	9 ± 43 <sup>e</sup>	0.50 ± 0.20 <sup>e</sup>			
SKOR	24	1.5	10-50	fair	98-04-01
SKOR	58	0.7	10-50	good	98-04-03
SKOR	17	1	10-50	good	98-05-21
SKOR	5	1.1	10-50	fair	98-05-22
SKOR	13	0.3	raw	fair	98-05-23
SKOR	4	0.6	raw	very good	98-06-07
SKOR	52	0.6	raw	good	98-08-20
SKOR	38	0.9	10-50	good	98-09-02
SKOR	3	1.5	10-50	fair	98-09-03
SKOR	38	0.6	raw	very good	98-12-27
SKOR	158	1	10-50	good	99-01-12
SKOR	158	0.4	raw	good	99-01-28
SKOR <sup>c</sup>	11 ± 26 <sup>e</sup>	0.85 ± 0.38 <sup>e</sup>			

<sup>a</sup>Orientation of the fast splitting direction in degree.

<sup>b</sup>Delay time between the two quasi-S waves in seconds.

<sup>c</sup>Filters give the signal bandpass in seconds.

<sup>d</sup>Null measurements.

<sup>e</sup>Mean (including only nonnull values).

deformation, this comparison will allow us to constrain models more easily than in wide regions of homogenous deformation such as Eurasia.

#### 4. Comparison With Structural Geology

The geological structure of the Aegean results in part from the stacking of different nappes atop one another, (from east to west) the Serbo-Macedonian, the Pelagonian, the Pindus, the

Gavrovro-Tripoliza, the Ionian, and the Preapulian zones, all of which collided successively since the Eocene with a shortening of several hundreds of kilometers and therefore implying not only the crust but also the upper mantle [Aubouin *et al.*, 1976; Jacobshagen, 1986]. These collisions were followed by rotations since the Lower Cenozoic, clockwise in the western Aegean and counterclockwise in the eastern Aegean [Kissel and Laj, 1988; Duermeijer, 1999]. Therefore the geological units and main structural sutures, which prior to rotation trended roughly EW, now trend NW-SE in continental Greece and WSW-ESE in

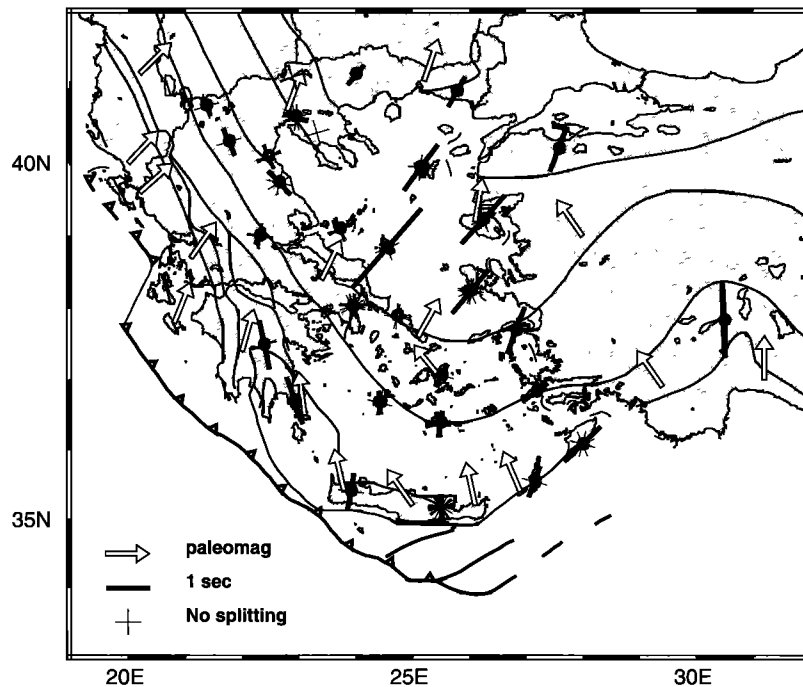


**Figure 4.** Map of the fast polarization direction of anisotropy superimposed on the geological map of the Aegean [after Robertson and Dixon, 1984]. This shows the weighted average (Tables 2 and 3) of the measurements for the stations computed in Table 1. We show the paleomagnetic rotations since the Miocene as measured by Duermeijer [1999]. No correlation between the observed directions of anisotropy and the rotation of the different geological units is observed indicating no relation between anisotropy and lithological fabric.

western Turkey (Figure 4). Because the different nappes consist of very different rock types (carbonates, limestones, flysch, and metamorphic), we might suspect that the observed anisotropy is related to the lithological fabric and the fast polarization orientation is inherited from the geological evolution of the Aegean. If this were the case, we should see some correlation between the fast polarization direction and the rotation of individual geological units. This hypothesis seems unlikely to us because the total amount of rotation is  $45^\circ$  clockwise in the west and  $25^\circ$  counterclockwise in the east, which has rotated the original structures to their present orientation of  $N135^\circ E$  in the west and  $N55^\circ E$  in the east, respectively (Figure 4). We do not see such a change in fast polarization direction between the west and the east. Furthermore, paleomagnetic rotations on Skiros are  $\sim 30^\circ$  clockwise, similar to continental Greece, while the fast polarization direction (which admittedly represents only one fair observation) is  $N45^\circ E$ , similar to the north Aegean Sea. It seems to us that the geological fabric, even rotated since the Late Cretaceous, cannot explain the orientation of anisotropy. The fast polarization directions are not parallel to the actual trend of the geological units and therefore are not related to lithological fabric exposed at the surface.

## 5. Comparison With Displacements Relative to the Lower Mantle

Since the late 1980s, many regional scale GPS campaigns have been conducted in and around the Aegean [e.g., Davies *et al.*, 1997; Clarke *et al.*, 1998; Kahle *et al.*, 1998; Reilinger *et al.*, 1997], and the inferred pattern of displacements relative to stable Eurasia is now well established [McClusky *et al.*, 2000]. All stations located north of the line connecting the North Aegean Trough and the Kefallinia fault (Figure 1) do not move significantly relative to stable Eurasia. On the other

hand, most of the stations located south of this line move approximately southwest at a velocity of  $\sim 3.0$  cm/yr. This first-order motion relative to Eurasia is quite well modeled as a rigid plate rotation of Anatolian around a pole located in Egypt near  $30^\circ N$ ,  $33^\circ E$  [Le Pichon *et al.*, 1995; Reilinger *et al.*, 1997]. The SW trending displacements relative to stable Europe decrease from 3 cm/yr along the north Anatolian fault toward the pole of rotation and are only  $\sim 1.6$  cm/yr near Rhodos. The fit between a small circle centered at the pole of rotation and the strike of the north Anatolian fault is good in the middle of the area, but it degrades at both ends, especially for the North Aegean Trough in the west [e.g., McClusky *et al.*, 2000].

Recent studies [e.g., Vinnik *et al.*, 1992, 1995] suggest that the lithosphere plate motion over the asthenosphere is the cause of anisotropy. In this case, the delay  $\delta t$  should be proportional to the velocity relative to the lower mantle and  $\Phi$  should be parallel to the motion of the lithospheric plates relative to an absolute frame. Knowing the motion of the Aegean relative to Eurasia [McClusky *et al.*, 2000], we computed the motion of the Aegean in the hot spot frame [Minster and Jordan, 1978] and in a no net rotation (NNR) frame [Argus and Gordon, 1991]. The motion of Eurasia in the hot spot frame is small ( $\sim 0.5$  cm/yr), but in a NNR frame it is of the same order ( $\sim 3$  cm/yr) as the motion of the Aegean relative to Eurasia.

We do not observe a similar pattern for the fast polarization parameters and the motion in the hot spot frame of Minster and Jordan [1978] (Figure 5). Indeed, the greatest values of splitting delays are observed south of the North Aegean Trough, but (1) the stations of AGGI and SKOP show little delay, even though located south of this line, (2)  $\Phi$  consistently trends NE-SW for the station located in Central Greece, contrary to the velocities, and (3) the splitting delays decrease toward the Hellenic trench systematically, especially around the sea of Crete, contrary to the velocity.

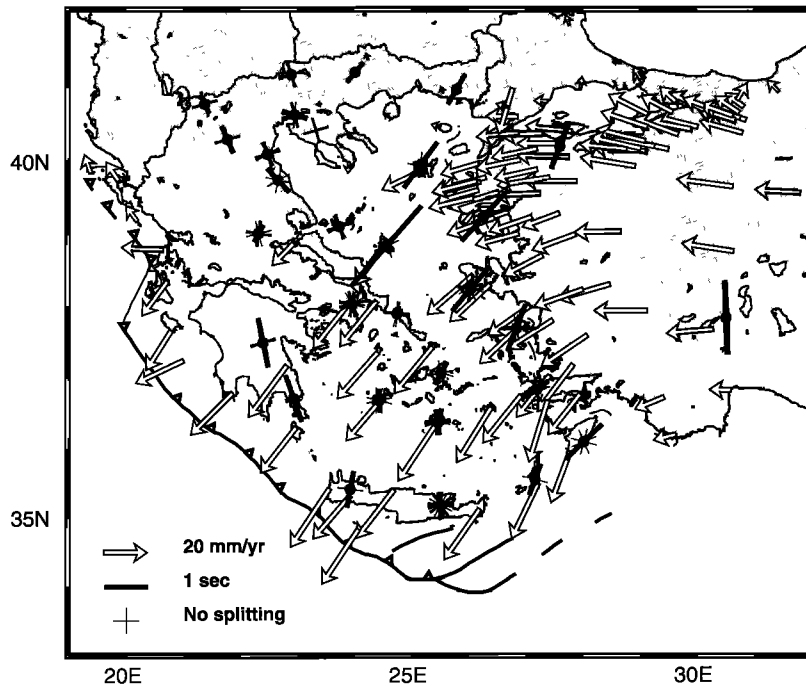


**Figure 5.** Map of the fast polarization direction of anisotropy (as in Figure 4) superimposed on the GPS displacement vectors computed in a hot spot frame [McClusky *et al.*, 2000; Minster and Jordan, 1978]. There is no clear relation between displacements and anisotropy.

In an NNR frame [Argus and Gordon, 1991] the velocity of the Aegean shows a complex pattern (Figure 6). There is no relation between both the directions and the amplitude of the velocities and anisotropy parameters. This is better demonstrated with a plot of

the delay times versus the velocities values in both absolute reference frame (Figure 7), which does not show any relationship between the motion of the upper plate relative to the asthenosphere and the anisotropy.

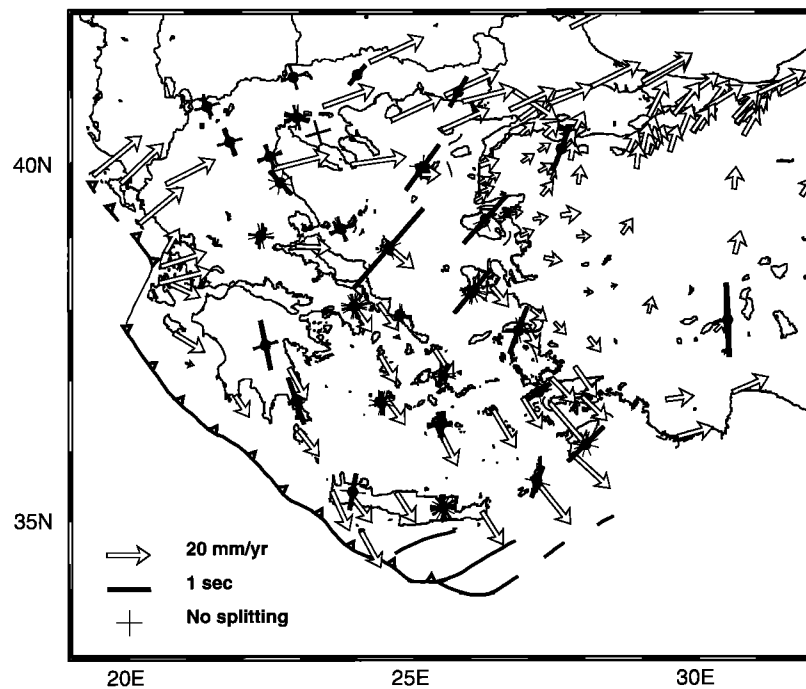


**Figure 6.** Map of the fast polarization direction of anisotropy (as in Figure 4) superimposed on the GPS displacement vectors computed in a no net rotation frame [McClusky *et al.*, 2000; Argus and Gordon, 1991]. There is no clear relation between displacements and anisotropy and hence no support for the asthenospheric flow hypothesis.

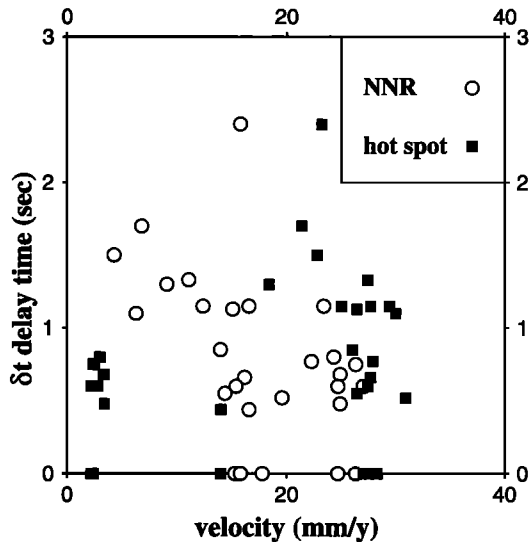


**Figure 7.** Delay times as a function of the GPS velocities (deduced from McClusky *et al.* [2000]) relative to a hot spot frame [Minster and Jordan, 1978] or to a no net rotation frame [Argus and Gordon, 1991]. It is not correlated with an increase of polarization delay time.

## 6. Comparison With Deformation Measurements

If we concentrate on the strain that affects the Aegean, excluding the Hellenic arc, extension trends homogeneously N-S within the Aegean, and some shortening is associated with the dextral strike-

slip motion of the North Aegean Trough [Jackson *et al.*, 1994; Papazachos *et al.*, 1998].

A more detailed examination of the displacement vectors [Le Pichon *et al.*, 1995; McClusky *et al.*, 2000] relative to the modeled motion of the rigid Anatolian plate shows (1) the observed displacements slightly diverge from the modeled displacements along the Hellenic Trench and (2) an increase of the displacements toward the Hellenic Trench (see also Figure 5). The misfit between observed and modeled displacements as well as the increase in velocity trenchward supports the idea that the Aegean region is deforming and is not a rigid block [e.g., McKenzie, 1978; Le Pichon and Angelier, 1979; Mercier *et al.*, 1989]. This internal deformation of the Aegean has been quantified by measuring velocities of geodetic benchmarks relative to each other, within the Aegean, and by the seismic energy released since the beginning of the century [Jackson *et al.*, 1994].

### 6.1. Seismicity

Earthquakes occur within the brittle part of the crust. Seismicity maps show that earthquakes are not homogeneously distributed over the Aegean (Figure 1) but are primarily located around the Hellenic Trench and western continental Greece and therefore related either to the active subduction or to the continental collision with Apulia. Earthquakes are also located in the north Aegean Sea and related to the north Anatolian fault. Several studies estimated the seismic energy release rate in the Aegean and compared it with the total deformation [Jackson and McKenzie, 1988; Ekström and England, 1989; Jackson *et al.*, 1994; Papazachos and Kiratzi, 1996]. In Figure 8 we show the seismic energy released, during the last century (which is also likely to be representative of longer period of time), as circles proportional to the seismic moment of each earthquake [Jackson *et al.*, 1992]. Most of the seismic energy release has occurred in the north Aegean Sea; only one strong earthquake (in 1956)

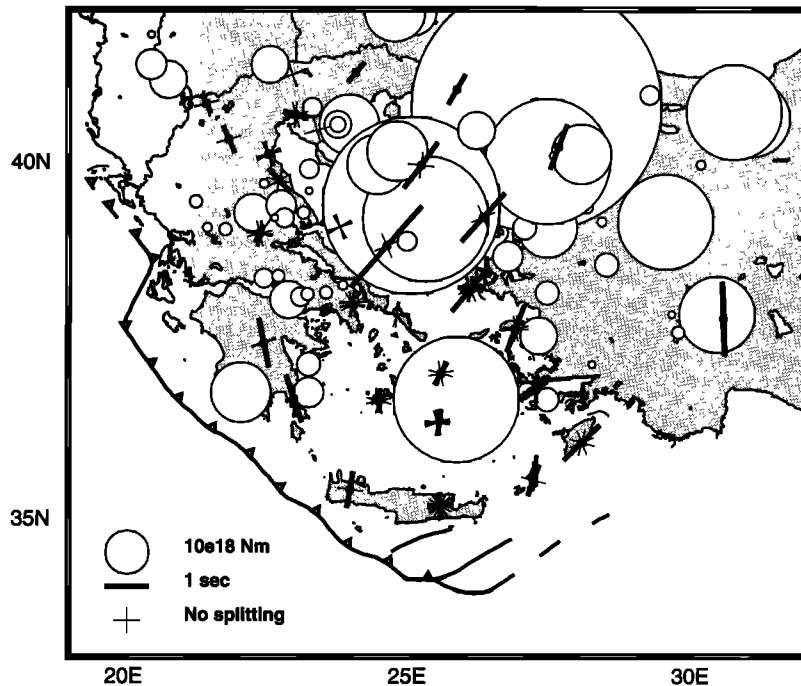


**Figure 8.** Map of the fast polarization direction of anisotropy (as in Figure 4) superimposed on the seismic energy release during the last century [Jackson *et al.*, 1992]. Circles are proportional to the seismic moment. Beside the Amorgos earthquake (36.7°N, 25.8°E), there is little seismic activity observed in the Sea of Crete where small anisotropy is observed.

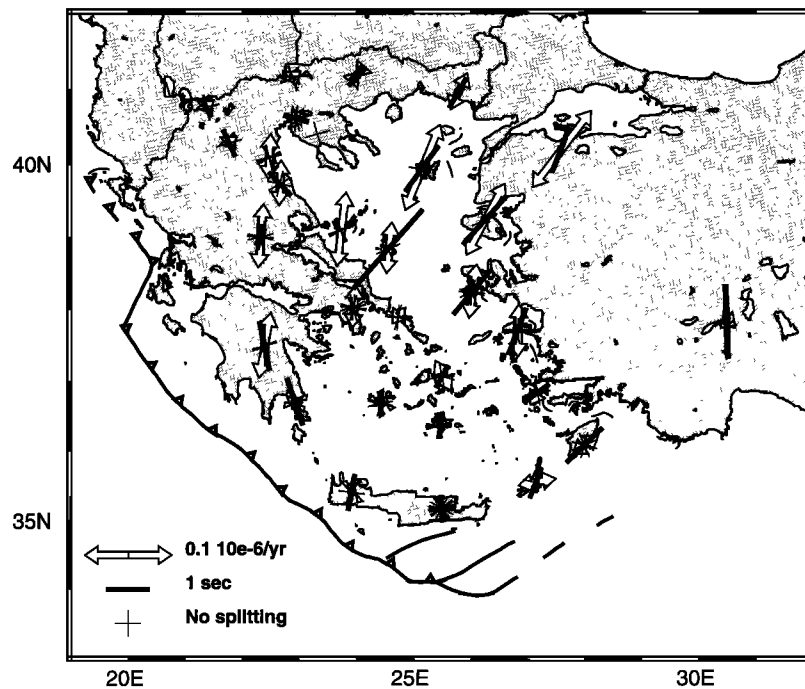


**Figure 9.** Map of the fast polarization direction of anisotropy (as in Figure 4) superimposed on the strain deduced from the GPS displacements [McClusky *et al.*, 2000]. The strain is computed for polygons of horizontal dimensions  $\sim 100$  km. The fit is better in the north Aegean Sea and western Turkey, suggesting that (1) the anisotropy is related to strain and (2) the upper mantle is deforming in a similar way to the shallow crust.

occurred in the Sea of Crete. Along the Hellenic Trench the relation between the total deformation and the seismic energy release could be biased because it seems to deform aseismically. However, this aseismic deformation relates only to the Hellenic subduction. As far as the Aegean Sea and continental Greece are concerned, the seismic energy release is well correlated with the total amount of deformation as it is deduced from satellite geodesy [Jackson *et al.*, 1994].

Thus it is clear that the seismic energy release is not homogenous over the Aegean. It is largest in the north Aegean Sea, where several earthquakes greater than magnitude 7 have occurred since the beginning of the century [Ambraseys and Jackson, 1990] but very much lower in the Sea of Crete, where only one magnitude 7 event has occurred near Amorgos. This difference in seismicity is also observed in the historical seismicity record [Papazachou and Papazachou, 1997].

Slip vectors from focal mechanisms give some information about the relative displacement between rigid blocks, and the  $P$  and  $T$  axes give some information about the strain regime. Both strong earthquakes [Ekström and England, 1989; Jackson *et al.*, 1994; Papazachou *et al.*, 1998] and microearthquakes [Hatzfeld *et al.*, 1997] show that the seismic energy released within the Aegean is consistent with N-S trending  $T$  axes in the north Aegean Sea. In contrast, extension is trending along the trench near the Hellenic arc.

## 6.2. Geodesy

The relative displacements of benchmarks measured by GPS also give an estimate of the internal deformation of the Aegean. The results of McClusky *et al.* [2000] are a synthesis of several campaigns conducted in the Aegean and western Turkey. From their results we first computed the deformation of triangles defined by three consecutive benchmarks. This gives unstable results because the triangles were not of uniform

dimensions and because in case of small triangles, uncertainties for one benchmark could lead to instabilities. We therefore computed the deformation over polygons centered around our seismological stations and of similar dimensions ( $\sim 100$  km) as the Fresnel zone of the SKS waves at a depth of 100 km. Figure 9 compares the mean anisotropy results in each station with the strain that affects such polygons centered on the station.

NNE-SSW extension is important in the north Aegean Sea from western Turkey to Greece, but it is smaller in continental Greece and in the south Aegean Sea. This deformation is not limited to the North Aegean Trough but also affects the islands of Samos (SAMO), Chios (HIOS), Lesbos (LESB), and Skiros (SKIR). Along the Hellenic arc the deformation is smaller and oriented in a different direction.

There is therefore some consistency between the amount of seismic energy release, the amount of internal deformation, and the value of the delay times observed for the SKS anisotropy (Figures 8 and 9). There is also a good correlation between the consistent NNE-SSW orientation of extension and  $\Phi$  in the northern Aegean. Finally, there is some agreement between the along-arc extension near the Hellenic arc and  $\Phi$  measured in the Peloponnese, Rhodes, and Karpathos.

## 7. Discussion

### 7.1. Cause of the Anisotropy

Crustal anisotropy is unable to explain SKS splitting time delays that are greater than a few tenths of a second [Crampin and Booth, 1985; McNamara *et al.*, 1994; Barruol and Mainprice, 1993]. On the other hand, mantle anisotropy due to strain that reorients minerals [Nicolas and Christensen, 1987; Mainprice and Silver, 1993; Silver, 1996] suggests that 1 s of splitting delay is due to anisotropy along paths of  $\sim 100$  km long,

**Table 4.** Comparison Between Anisotropy Parameters and Deformation Parameters Deduced From GPS Measurements<sup>a</sup>

Station	$\Phi^b$	$\sigma\Phi$	$\delta^c$	$\sigma\delta$	$\epsilon_{11}/\gamma^d$	$\theta^e$	$\Phi-\theta$
AGGI	28	10	0.44	0.13	73	5	23
ALEX	30	13	0.8	0.15	46	25	5
ANAT	137	18	0.75	0.35	52	3	-46
ANDR	fair null	...	...	...	24	40	...
BAND	21	45	1.1	0.5	110	37	-16
HIOS	40	26	1.33	0.29	62	8	32
DRAM	40	17	0.6	0.3	6	41	-1
FLOR	154	9	0.48	0.09	20	141	13
ISPA	177	13	1.7	0.35	24	135	42
KARP	21	14	0.77	0.23	43	79	-58
KENT	fair null	...	...	...	20	141	...
KOSI	54	14	0.66	0.18	35	32	22
KOZA	156	10	0.68	0.22	20	141	15
KRIS	good null	...	...	...	37	43	...
LESB	42	6	1.5	0.18	92	28	14
LIMN	36	11	1.3	0.23	106	22	14
LITO	fair null	...	...	...	52	3	...
MILO	175	12	0.55	0.25	5	148	27
NAXO	30	22	0.6	0.26	38	153	57
PENT	fair null	...	...	...	48	4	...
RODO	46	10	1.15	0.18	36	53	-7
SAMO	21	2	1.15	0.09	60	1	20
SANT	9	43	0.52	0.2	16	130	59
SKIR	41	15	2.4	0.6	58	6	35
SKOP	good null	...	...	...	85	7	...
SKOR	11	26	0.85	0.38	3	170	21
THES	107	45	0.6	0.5	21	152	-45
TRIP	168	45	1.15	0.5	75	10	-19
VAVD	fair null	...	...	...	21	152	...
VELI	161	9	1.13	0.18	7	102	58

<sup>a</sup> See McClusky *et al.* [2000].

<sup>b</sup> Orientation of the fast splitting direction in degree (see Tables 2 and 3).

<sup>c</sup> Delay time (s) between the two quasi-S waves in seconds (see Tables 2 and 3).

<sup>d</sup> Annual strain rate ( $10^{-9}$ ) deduced from GPS measurements.

<sup>e</sup> Orientation of the maximum extension in degree relative to north.

implying anisotropy through the whole lithosphere and possibly the asthenosphere. Our observations show SKS splitting delays of up to 2 s and therefore suggest that both the whole lithosphere and part of the asthenosphere are involved in the process that splits the observed SKS waves; this is especially true for the northern Aegean Sea. In the case of the southern Aegean and, especially, along the Hellenic arc the horizontal anisotropy could be blurred by the subduction of the African lithospheric plate beneath the Hellenic arc because the asthenospheric flow is certainly complex.

There is no correlation of  $\Phi$  with the NW-SE trend of the geological unit or with the paleomagnetic rotations that occurred after the middle Miocene or during the Quaternary [Kissel and Laj, 1988; Duermeijer, 1999], nor is there a correlation with the amount of total deformation that affected the Aegean since the middle Miocene because anisotropy is not seen in the Sea of Crete (stations NAXO, SANT, and MILO), which experienced a stretching factor of  $\sim 2$  [Angelier *et al.*, 1982]. Thus our observations show that the fast polarization direction is probably not related to the geological fabric or inherited tectonical processes.

The orientation of anisotropy does not align with the orientation of displacement of the Aegean relative to any of the hot spot or NNR frames, and the splitting delay times do not correlate with the displacement velocities (Figure 7). Thus it seems unlikely that anisotropy is due to the rigid plate tectonic motion relative to an absolute reference frame. If we consider the motion relative to a hot spot frame,  $\Phi$  should align with the motion of the Peloponnese. In a NNR frame we should observe a large delay time in central and northern Greece. Therefore our fast polarization directions do not support the simple asthenospheric flow model [e.g., Vinnik *et al.*,

1995], which assumes that anisotropy is controlled by the absolute plate motion.

Our fast polarization direction does not align with the orientation of the major crustal (or lithospheric) discontinuities (i.e., the different branches of the North Aegean Trough). Any interpretation in terms of vertically coherent deformation [see Silver, 1996] as it has been proposed for the north Kunlun fault [e.g., McNamara *et al.*, 1994] is not supported by our observations. In the north Kunlun fault the fast polarization direction rotates quickly to become parallel to the fault, and values of delay times also vary rapidly with the distance to the fault. In the Aegean,  $\Phi$  does not align with the North Aegean Trough in ALEX, LESB, and BAND, and the amplitude of the delay is rather constant from ALEX to SKIR and SAMO. It seems therefore unlikely that anisotropy is restricted to the major crustal (or lithospheric) discontinuities.

On the other hand, the pattern of fast polarization direction closely resembles the pattern of extensional strain inferred both from the geodetic measurements [e.g., Davies *et al.*, 1997; Kahle *et al.*, 1998] and the  $T$  axes of focal mechanisms [Hatzfeld *et al.*, 1997]. It trends uniformly NNE-SSW over most of the northern Aegean, and it is aligned with the Hellenic Trench in the Peloponnese, Rhodos, and Karpathos. It is not limited to the North Aegean Trough but affects a broad region from ALEX to SAMO. The delay time correlates reasonably well with the amount of seismic energy release (Figure 8), and the orientation correlates with the mean direction of extension (Figure 9). It seems probable that the SKS splitting is therefore related to the current strain rate (or recent finite strain) rather than the total amount of finite deformation over a long time. The agreement is good in the northern

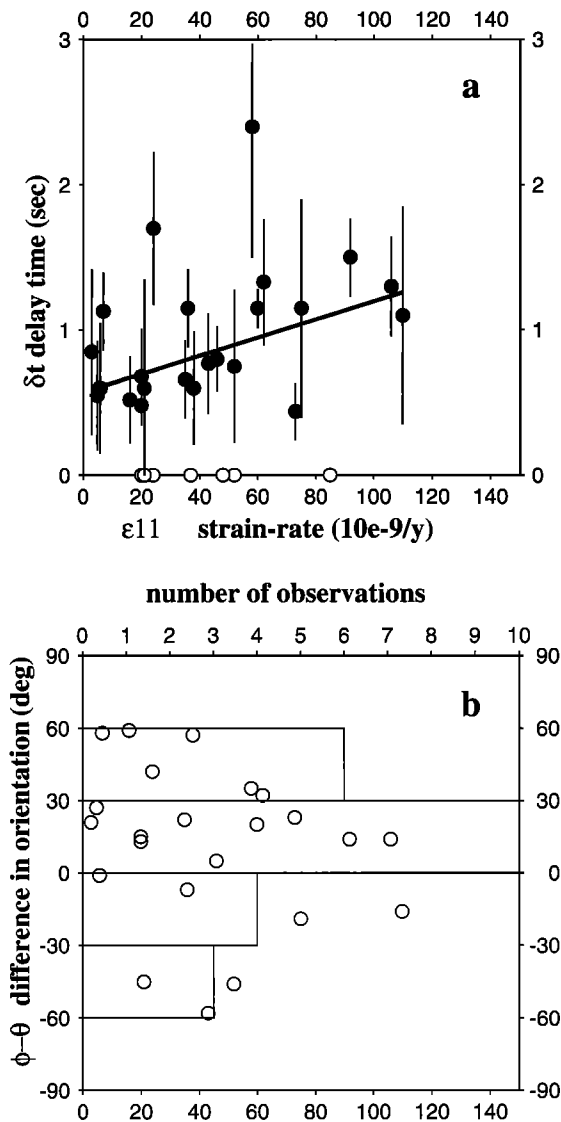


**Figure 10.** (a) Delay times as a function of the strain rate deduced from GPS measurements. The thick line represents the least squares weighted fit. Solid dots are the weighted average of individual measurements and vertical bars are uncertainties (Tables 2 and 3). The intercept at zero strain could represent the crustal contribution to anisotropy and is also the average uncertainty of the measurements. (b) Difference in the orientation of the splitting direction and the direction of maximum extension versus the strain rate (Table 4). For small values of the strain rate the scatter is important (but not random), while for large values the scatter is  $<30^\circ$ . The histogram of the measurements (scale at the top) shows a maximum between  $0^\circ$  and  $30^\circ$  of orientation shift.

Aegean Sea. Along the Hellenic arc, mainly for the Peloponnese, Rhodes, and Karpathos, the fast polarization direction agrees with the direction of extensional strain as it is deduced from earthquake mechanisms but does not agree with the delay times. It is important to note that the Hellenic subduction is rather peculiar and dips at a very shallow angle beneath the Peloponnese. On the other hand, the fast polarization direction above some subduction zones has been observed parallel to the trench [e.g., Russo and Silver, 1994]. Beneath the Peloponnese, both effects could constructively interfere, while they destructively interfere beneath Crete.

## 7.2. Implication for the Geodynamics

Anisotropy in the Aegean is not restricted to the major faults but is distributed within a wide region around the major discontinuities which are represented by the different branches of the North Aegean Trough. This result is similar to the observations in New Zealand [e.g., Molnar *et al.*, 1999] or in Tibet [e.g., Davis *et al.*, 1997; Holt, 2000].

If we assume that surface faults are crustal discontinuities but that the mantle lithosphere deforms continuously beneath the crust, we can estimate the amount of strain that affects the lithosphere. A rough estimate of the total motion of Anatolia relative to Eurasia along the north Anatolian fault is  $\sim 80\text{--}100$  km since the Pliocene [i.e., Barka and Hancock, 1984]. Assuming a simple-shear deformation by displacement  $d = 100$  km affecting a region of width  $w = 100$  km (the width of the different branches of the North Aegean Trough), we compute an angle  $\theta = 30^\circ$  between the direction of the maximum extension and the direction of shear, and we compute a finite strain of  $\varepsilon_{11} = 60\%$ . First,  $30^\circ$  is approximately the angle between  $\Phi$  and the direction of motion along the North Aegean Trough. Second, a finite strain of 60% produces an anisotropy  $\delta v_s/v_s = 7\%$  [Ribe, 1992], which is consistent with a time delay of 2 s for a wave propagation over 100 km. Moreover, the present-day observed geodetic strain rate is  $\sim 0.06\text{--}0.1 \cdot 10^{-6}/\text{yr}$  in the region of high anisotropy located in the north Aegean Sea around the stations (Table 4). Accumulated over a period of 5 Myr, this contributes to a total finite strain of 30–50%, which, again, is consistent with the anisotropy values computed above.

From the GPS velocities reported by McClusky *et al.* [2000] we computed the strain rate  $\varepsilon_{11}$  of a polygon centered on each station and of dimension  $\sim 100$  km (Table 4). For each polygon we compare (1) the difference  $\Phi - \theta$  between the direction of fast polarization and the direction of GPS strain extension and (2) the delay time  $\delta t$ , with the extension rate  $\varepsilon_{11}$ . This comparison is shown in Figure 10. The difference  $\Phi - \theta$  in orientation is quite scattered but is not random, and clearly, the scatter is less for large strain rates beyond the noise. We observe that the distribution of  $\theta - \Phi$  is centered between  $0^\circ$  and  $30^\circ$ , but we have no obvious explanation for this. The values of the delay time  $\delta t$  correlate also with the strain rates even when the scatter is large. The intercept at zero strain rate is of  $\sim 0.5$  s, which is a reasonable value for anisotropy possibly due to the crust. All values are also associated with uncertainties equal or larger than 0.5 s. This could be considered as noise added to the data and strengthen the link between the value of the delay time and the geodetic strain.

These correlations imply that anisotropy (and delay time) are related to the strain measured at the surface and that deformation affects the upper mantle. That is, the instantaneous deformation pattern observed at the surface with GPS measurements is similar to the anisotropy pattern, which is due to finite strain of the upper mantle during a certain duration of time. This is similar to the conclusions inferred both from measurements conducted in New Zealand [e.g., Molnar *et al.*, 1999] or in Tibet [Davis *et al.*, 1997; Holt, 2000]. All these interpretations correlate the anisotropy with the deformation of the crust and upper mantle, supporting vertically coherent deformation. The interpretation differs in that the direction of extension of finite strain during a certain amount of time (the Cenozoic) is invoked in one interpretation [Davis *et al.*, 1997], while present-day plane of shear is invoked in another [Holt, 2000]. In our case, the anisotropy correlates well with the present-day extension, which we assume is constant during the Pliocene but differs significantly from previous deformation. The Pliocene finite strain in our case is  $\sim 60\%$ , while it was greater in Tibet. Zhang and Karato [1995] have shown that for finite strain of the order of 100% the fast polarization direction rotates to become parallel to the shear plane, which could reconcile the observations for Tibet and for the Aegean. This lithospheric deformation is not restricted to the major surface discontinuities (the North Aegean

Trough) but is spread over a wide region. This suggests that the upper mantle deforms in a continuum fashion and that different branches of the North Aegean Trough are only the brittle surface expression of the mantle deformation.

## 8. Conclusion

The Aegean experiences significant present-day internal deformation. Unlike most of the places where anisotropy has been measured, the Aegean strain rate is large and implies a large two-dimensional strain pattern. Measurements of mantle anisotropy in the Aegean do not correlate with preexisting structural fabric (frozen into the lithosphere). Nor do they correlate with geodetic displacements relative to absolute plate motion and therefore do not fit models which involve the upper mantle in the plate motion. They do not align well with the major transcurrent faults of the North Aegean Trough and are therefore inconsistent with models that predict that anisotropy is related to the horizontal motion of the lithosphere over a mantle asthenosphere.

On the other hand, the fast polarization parameters are rather well correlated, both in terms of orientation and magnitude, with the recent strain rates as evidenced by the GPS measurements and the seismicity (energy release and focal mechanisms). It is spread over a wide region around the major faults. Values of delay time are too large to be restricted to the path in the crust and therefore suggest that the crust and upper mantle deform similarly.

**Acknowledgments.** This study was supported by contract ENV4-C196-0277 from the program Environment and Climate of the European Commission and the program IDYL of INSU-CNRS. We thank all the observers who helped us to maintain the stations during the six months of the experiment. P. Clarke and J.-C. Ruegg kindly provided the programs to compute the strain from GPS measurements and the change in reference frame. J. Jackson, P. England, and P. Molnar provided helpful comments on earlier versions of the manuscript. G. Helffrich (Associate Editor), W. Holt, and an anonymous reviewer gave constructive criticisms, which greatly improve the manuscript.

## References

- Alsina, D., and R. Snieder, Small-scale sublithospheric continental mantle deformation: Constraints from SKS splitting observations, *Geophys. J. Int.*, **123**, 431–448, 1995.
- Ambraseys, N., and J. Jackson, Seismicity and associated strain of central Greece between 1890 and 1988, *Geophys. J. Int.*, **101**, 663–708, 1990.
- Angelier, J., N. Lyberis, X. Le Pichon, E. Barrier, and P. Huchon, The neotectonic development of the Hellenic Arc and the Sea of Crete: A synthesis, *Tectonophysics*, **86**, 159–196, 1982.
- Argus, D. F., and P. G. Gordon, No-net-rotation model of current plate velocities incorporating plate motion model Nuvel-1, *Geophys. Res. Lett.*, **18**, 2039–2042, 1991.
- Aubouin, J., M. Bonneau, J. Davidson, P. Leboulanger, S. Matesco, and A. Zambetakis, Esquisse structurale de l'arc Égéen externe: Des Dinarides aux Taurides, *Bull. Soc. Géol. Fr.*, **7**, 385–401, 1976.
- Barka, A. A., and P. L. Hancock, Neotectonic deformation patterns in the convex-northwards arc of the north Anatolian fault zone, in *The Geological Evolution of the Eastern Mediterranean*, edited by J. E. Dixon and A. H. F. Robertson, *Geol. Soc. Spec. Publ.*, **17**, 763–774, 1984.
- Barruol, G., and D. Mainprice, A quantitative evaluation of the contribution of crustal rocks to shear wave splitting of teleseismic SKS waves, *Phys. Earth Planet. Inter.*, **78**, 281–300, 1993.
- Ben Ismail, W., and D. Mainprice, An olivine fabric database: An overview of upper mantle fabrics and seismic anisotropy, *Tectonophysics*, **296**, 145–157, 1998.
- Bourne, S. J., P. C. England, and B. Parsons, The motion of crustal blocks driven by flow of the lithosphere: Implications for slip rates of faults in the South Islands of New Zealand and southern California, *Nature*, **391**, 655–659, 1997.
- Clarke, P. J., et al., Crustal strain in central Greece from repeated GPS measurements in the interval 1989–1997, *Geophys. J. Int.*, **135**, 195–214, 1998.
- Crampin, S., and D. C. Booth, Shear-wave polarizations near the north Anatolian fault, II, Interpretation in terms of crack-induced anisotropy, *Geophys. J. R. Astron. Soc.*, **83**, 75–92, 1985.
- Davies, R., P. England, B. Parsons, H. Billiris, D. Paradissis, and G. Veis, Geodetic strain of Greece in the interval 1892–1992, *J. Geophys. Res.*, **102**, 24,571–24,588, 1997.
- Davis, P., P. England, and G. Houseman, Comparison of shear wave splitting and finite strain from the India-Asia collision zone, *J. Geophys. Res.*, **102**, 27,511–27,522, 1997.
- Duermeijer, C. E., Neogene to Recent tectonic evolution of the central Mediterranean, an integrated paleomagnetic approach, Ph.D. thesis, Utrecht, Netherlands, 1999.
- Ekström, G., and P. England, Seismic strain rates in regions of distributed continental deformation, *J. Geophys. Res.*, **94**, 10,231–10,257, 1989.
- England, P., and D. McKenzie, A thin viscous sheet model for continental deformation, *Geophys. J. R. Astron. Soc.*, **70**, 295–321, 1982.
- England, P., G. Houseman, and L. Sonder, Length scales for continental deformation in convergent, divergent, and strike slip environments: Analytical and approximate solutions for a thin viscous sheet model, *J. Geophys. Res.*, **90**, 3551–3557, 1985.
- Farra, V., L. P. Vinnik, B. Romanowicz, G. L. Kozarev, and R. Kind, Inversion of teleseismic S particle motion for azimuthal anisotropy in the upper mantle: A feasibility study, *Geophys. J. Int.*, **106**, 421–431, 1991.
- Hatzfeld, D., J. Martinod, G. Bastet, and P. Gautier, An analog experiment for the Aegean to describe the contribution of gravitational potential energy, *J. Geophys. Res.*, **102**, 649–659, 1997.
- Holt, W. E., Correlated crust and mantle strain fields in Tibet, *Geology*, **28**, 67–70, 2000.
- Jackson, J. A., and D. McKenzie, The relationship between plate motions and seismic moment tensors, and the rates of active deformation in the Mediterranean and the Middle East, *Geophys. J.*, **93**, 45–73, 1988.
- Jackson, J., J. Haines, and W. Holt, The horizontal velocity field in the deforming Aegean Sea region determined from the moment tensors of earthquakes, *J. Geophys. Res.*, **97**, 17,657–17,684, 1992.
- Jackson, J., J. Haines, and W. Holt, A comparison of satellite laser ranging and seismicity data in the Aegean region, *Geophys. Res. Lett.*, **21**, 2849–2852, 1994.
- Jacobshagen, V., *Geologie von Griechenland*, 363 pp., Gebrüder Borntraeger, Stuttgart, Germany, 1986.
- Kahle, H.-G., C. Straub, R. Reilinger, S. McClusky, R. King, K. Hurst, G. Veis, K. Kastens, and P. Cross, The strain field in the eastern Mediterranean region, estimated by repeated GPS measurements, *Tectonophysics*, **294**, 237–252, 1998.
- Kissel, C., and C. Laj, The tertiary geodynamical evolution of the Aegean arc: A paleomagnetic reconstruction, *Tectonophysics*, **146**, 183–201, 1988.
- Le Pichon, X., and J. Angelier, The Hellenic arc and trench system: A key to the neotectonic evolution of the eastern Mediterranean region, *Tectonophysics*, **60**, 1–42, 1979.
- Le Pichon, X., N. Chamot-Rooke, S. Lallemand, R. Noomen, and G. Veis, Geodetic determination of the kinematics of central Greece with respect to Europe: Implications for eastern Mediterranean tectonics, *J. Geophys. Res.*, **100**, 12,675–12,690, 1995.
- Mainprice, D., and P. G. Silver, Interpretation of SKS waves using samples from the subcontinental lithosphere, *Phys. Earth Planet. Inter.*, **78**, 257–280, 1993.
- McClusky, S., et al., GPS constraints on plate motions and deformations in the eastern Mediterranean: Implications for plate dynamics, *J. Geophys. Res.*, **105**, 5695–5719, 2000.
- McKenzie, D. P., Active tectonics of the Alpine-Himalayan belt: The Aegean Sea and surrounding regions, *Geophys. J. R. Astron. Soc.*, **55**, 217–254, 1978.
- McNamara, D. E., T. J. Owens, P. G. Silver, and F. T. Wu, Shear wave anisotropy beneath the Tibetan Plateau, *J. Geophys. Res.*, **99**, 13,655–13,665, 1994.
- Meijer, P. T., and M. J. R. Wortel, Present-day dynamics of the Aegean region: A model analysis of the horizontal pattern of stress and deformation, *Tectonics*, **16**, 879–895, 1997.
- Mercier, J. L., D. Sorel, P. Vergely, and K. Simeakis, Extensional tectonic regimes in the Aegean basins during the Cenozoic, *Basin Res.*, **2**, 49–71, 1989.
- Minster, J. B., and T. H. Jordan, Present-day plate motion, *J. Geophys. Res.*, **83**, 5331–5354, 1978.
- Molnar, P., Continental tectonics in the aftermath of plate tectonics, *Nature*, **335**, 131–137, 1988.
- Molnar, P., et al., Continuous deformation versus faulting through the continental lithosphere of New Zealand, *Science*, **286**, 516–519, 1999.
- Nicolas, A., and N. I. Christensen, Formation and anisotropy in upper mantle peridotites — A review, in *Composition, Structure, and Dynamics of the Lithosphere — Asthenosphere System*, *Geodyn. Ser.*, vol. 16, edited by K. Fuchs and C. Froidevaux, pp. 111–123, AGU, Washington, D. C., 1987.

- Nur, A., H. Ron, and O. Scotti, Fault mechanics and the kinematics of block rotation, *Geology*, *14*, 746–749, 1986.
- Papazachos, B., and K. Papazachou, *Earthquakes in Greece*, 356 pp., Ekdoiseis Ziti, Thessaloniki, Greece, 1997.
- Papazachos, B. C., E. E. Papadimitriou, A. A. Kiratzi, C. B. Papazachos, and E. K. Louvari, Fault plane solutions in the Aegean Sea and the surrounding area and their tectonic implication, *Boll. Geof. Teorica Appl.*, *39*, 199–218, 1998.
- Papazachos, C. B., and A. A. Kiratzi, A detailed study of the active crustal deformation in the Aegean and surrounding area, *Tectonophysics*, *253*, 129–153, 1996.
- Reilinger, R., S. C. McClusky, M. B. Oral, R. W. King, and M. N. Toksoz, Global Positioning System measurements of present-day crustal movements in the Arabia-Africa-Eurasia plate collision zone, *J. Geophys. Res.*, *102*, 9983–9999, 1997.
- Ribe, N. M., On the relation between seismic anisotropy and finite strain, *J. Geophys. Res.*, *97*, 8737–8747, 1992.
- Robertson, A. H. F., and J. E. Dixon, Introduction: Aspects of the geological evolution of the eastern Mediterranean, in *The Geological Evolution of the Eastern Mediterranean*, edited by J. E. Dixon and A. H. F. Robertson, *Geol. Soc. Spec. Publ.*, *17*, 1–74, 1984.
- Russo, R. M., and P. G. Silver, Trench-parallel flow beneath the Nazca plate from seismic anisotropy, *Science*, *263*, 1105–1111, 1994.
- Silver, P. G., Seismic anisotropy beneath the continents: Probing the depths of the geology, *Annu. Rev. Earth Planet. Sci.*, *24*, 385–432, 1996.
- Silver, P. G., and W. W. Chan, Shear wave splitting and subcontinental mantle deformation, *J. Geophys. Res.*, *96*, 16,429–16,454, 1991.
- Tapponnier, P., Evolution tectonique du système alpin en Méditerranée. Poinçonnement et écrasement rigide plastique, *Bull. Soc. Géol. Fr.*, *3*, 437–460, 1977.
- Tapponnier, P., G. Peltzer, and R. Armijo, On the mechanics of the collision between India and Asia, in *Collision Tectonics*, edited by M. P. Coward and A. C. Ries, *Geol. Soc. Spec. Publ.*, *19*, 115–157, 1986.
- Tommasi, A., A. Vauchez, and R. Russo, Seismic anisotropy in ocean basins: Resistive drag of the sub-lithospheric mantle?, *Geophys. Res. Lett.*, *23*, 2991–2994, 1996.
- Vinnik, L. P., V. Farra, and B. Romanowicz, Azimuthal anisotropy in the Earth from observations of SKS at Geoscope and Nars broadband stations, *Bull. Seismol. Soc. Am.*, *79*, 1542–1558, 1989.
- Vinnik, L. P., L. I. Makeyeva, A. Milev, and A. Y. Usenko, Global patterns of azimuthal anisotropy and deformations in the continental mantle, *Geophys. J. Int.*, *111*, 433–447, 1992.
- Vinnik, L. P., R. W. Green, and B. Gruzinskaya, Recent deformation of the deep continental root beneath southern Africa, *Nature*, *375*, 50–52, 1995.
- Wylegalla, K., G. Bock, J. Gossler, and W. Hanka, Anisotropy across the Sorgenfrei-Tornquist zone from shear wave splitting, *Tectonophysics*, *314*, 335–350, 1999.
- Zhang, S., and S.-I. Karato, Lattice preferred orientation of olivine aggregates deformed in simple shear, *Nature*, *375*, 774–777, 1995.
- 
- G. Bock, GeoForschungsZentrum Potsdam, Telegrafenberg, 14473 Potsdam, Germany.
- D. Hatzfeld, Laboratoire de Géophysique Interne et Tectonophysique, UJF-CNRS, BP 53, 38041 Grenoble Cedex, France. (denis.hatzfeld@ujf-grenoble.fr)
- E. Karagianni, A. Kiratzi, and E. Louvari, Department of Geophysics, Aristotle University, BP 352-01, 54006 Thessaloniki, Greece.
- I. Kassaras, K. Makropoulos, and P. Papadimitriou, Department of Geophysics, University of Athens, Ilissia, 15784 Athens, Greece.
- H. Lyon-Caen, Laboratoire de Géologie, Ecole Normale Supérieure, 75231 Paris Cedex 05, France.
- K. Priestley, Bullard Laboratory, Madingley Rise, Madingley Road, Cambridge CB30EZ, England, UK.

(Received March 23, 2000; revised July 1, 2001; accepted July 5, 2001.)